Supporting Information

Aluminum Methyl, Alkoxide and α-Alkoxy Ester Complexes Supported by 6,6'-Dimethylbiphenyl-Bridged Salen Ligands: Synthesis, Characterization and Catalysis for *rac*-Lactide Polymerization

Chao Kan, Jilei Ge and Haiyan Ma*

Shanghai Key Laboratory of Functional Materials Chemistry and Laboratory of Organometallic Chemistry, East China University of Science and Technology, 130 Meilong Road, Shanghai 200237, P. R. China

* To whom correspondence should be addressed. Tel./Fax: +86 21 64253519.

E-mail: haiyanma@ecust.edu.cn.

Table of contents

Figure S34. ^{1}H NMR spectrum of the NMR tube reactions of complex **5** and one equiv. of ^{i}PrOH in the presence of 20 equiv. of *rac*-LA.

5. Kinetic studies

Figure S35. Relationship of M_n and the polydispersity index (PDI) of the PLA sample versus monomer conversion catalyzed by complex **2**/^{i}PrOH.

Figure S36. Semilogarithmic plots for the polymerization of *rac*-LA promoted by complexes **1**−**3**.

Figure S37. A) Semilogarithmic plots of ln([LA]$_0$/[LA]$_t$) versus time catalyzed by complex **8**; B) Linear plot of lnk_{obs} versus ln[Al] for the polymerization of *rac*-LA using **8** as an initiator.

6. Microstructure Analysis of Polylactides

Figure S38. ^{1}H NMR spectrum of the *rac*-LA oligomer produced by complex **8**.

Figure S39. ESI-TOF mass spectrum of the *rac*-LA oligomer produced by complex **8**.

Figure S40. Homonuclear decoupled ^{1}H NMR spectrum of PLA produced from *rac*-LA using complex **1**/^{i}PrOH as initiator.

Figure S41. ESI-TOF mass spectrum of the *rac*-LA oligomer produced by complex **4** ([*rac*-LA] : [**4**] = 20:1, in toluene).

Figure S42. Homonuclear decoupled ^{1}H NMR spectrum of PLA produced from *rac*-LA using complex **4** as initiator.

1. Molecular structures

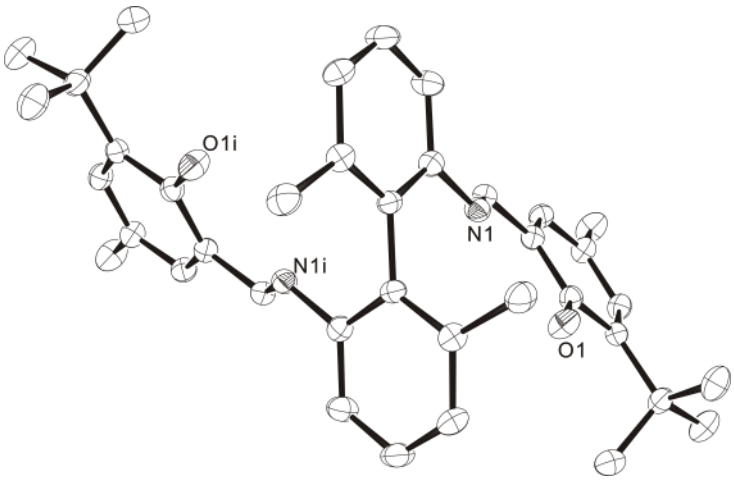

Figure S1. Molecular structure of proligand $\mathbf{L^2H_2}$ (all hydrogen atoms omitted for clarity; thermal ellipsoids drawn at the 50% probability level).

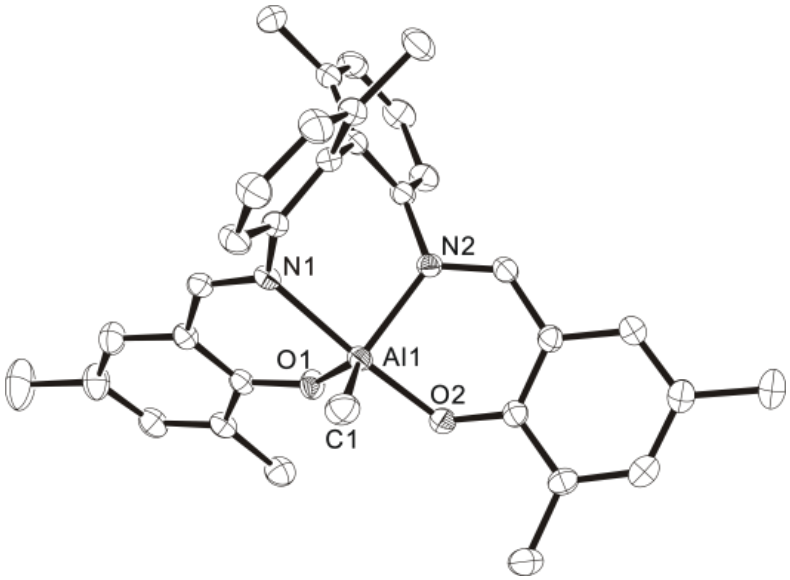

Figure S2. Molecular structure of **1** (all solvent molecules and hydrogen atoms omitted for clarity; thermal ellipsoids drawn at the 50% probability level). Selected bond lengths (Å) and angles (deg): Al1–O1 1.7733(12), Al1–O2 1.8340(12), Al1–N1 2.1142(14), Al1–N2 2.0165(13), Al1–C1 1.9771(18), O1–Al1–O2 91.99(6), O1–Al1–N1 87.62(6), O1–Al1–N2 112.94(6), O2–Al1–N1 175.09(6), O2–Al1–N2 88.68(5), O1–Al1–C1 125.06(7), O2–Al1–C1 93.42(7), N2–Al1–N1 86.96(5), C1–Al1–N1 90.81(7), C1–Al1–N2 121.81(7).

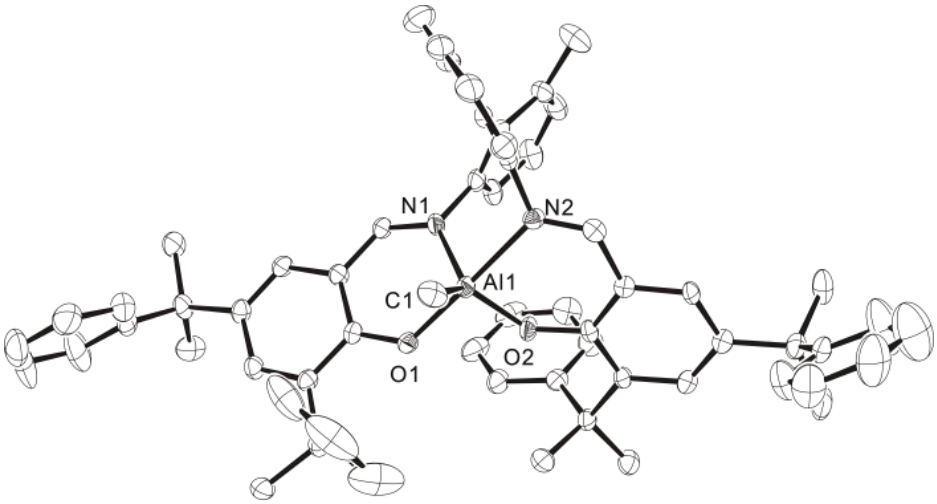

Figure S3. Molecular structure of **3** (all hydrogen atoms omitted for clarity; thermal ellipsoids drawn at the 50% probability level). Selected bond lengths (Å) and angles (deg): Al1–O1 1.852(2), Al1–O2 1.773(2), Al1–N1 1.990(3), Al1–N2 2.112(3), Al1–C1 1.935(4), O1–Al1–O2 92.10(11), O1–Al1–N1 89.29(11), O1–Al1–N2 176.79(11), O2–Al1–N1 109.22(12), O2–Al1–N2 87.48(11), O1–Al1–C1 93.01(14), O2–Al1–C1 127.42(15), N1–Al1–N2 87.85(11), C1–Al1–N1 123.14(15), C1–Al1–N2 89.77(14).

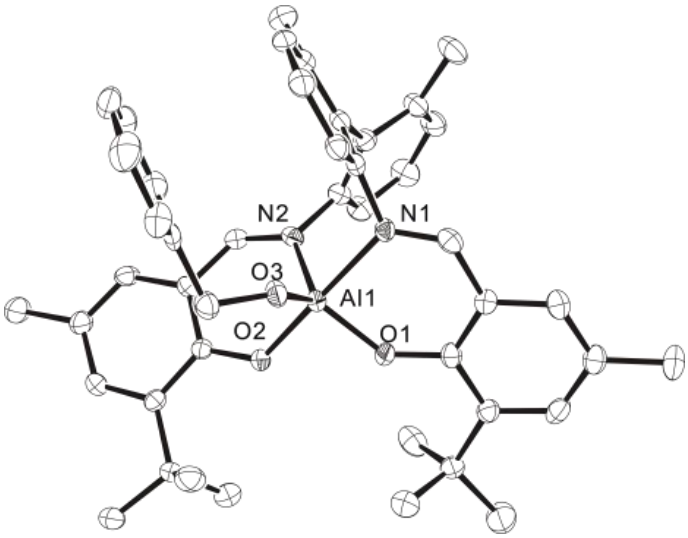

Figure 4. Molecular structure of **9** (all hydrogen atoms omitted for clarity; thermal ellipsoids drawn at the 50% probability level). Selected bond lengths (Å) and angles (deg): Al1–O1 1.758(2), Al1–O2 1.816(2), Al1–O3 1.729(2), Al1–N1 2.044(3), Al1–N2 1.992(3), O1–Al1–O2 90.19(11), O1–Al1–O3 123.80(11), O2–Al1–O3 99.75(12), O1–Al1–N1 88.08(11), O2–Al1–N1 174.58(12), O3–Al1–N1 85.48(12), O1–Al1–N2 116.99(13), O2–Al1–N2 88.32(11), O3–Al1–N2 118.46(12), N1–Al1–N2 87.89(12).

2. Crystallographic data

Table S1. Crystallographic data for proligand **L^2H_2**, complexes **1** and **2**

	L^2H_2	**1**	**2**
Empirical formula	$C_{38}H_{44}N_2O_2$	$C_{36}H_{36}AlN_2O_2$	$C_{39}H_{45}AlN_2O_2$
Formula weight	560.75	555.65	600.75
Temp (K)	130	140(2)	140(2)
Wavelength (Å)	0.71073	0.71073	0.71073
Crystal system	Orthorhombic	Monoclinic	Monoclinic
Space group	A e a 2	C 2/c	C 2/c
a (Å)	9.9750(19)	28.105(3)	29.421(5)
b (Å)	30.060(7)	12.8850(15)	11.873(2)
c (Å)	10.719(2)	17.816(2)	20.751(4)
α (°)	90	90	90
β (°)	90	108.596(2)	109.235(3)
γ (°)	90	90	90
Volume ($Å^3$)	3214.0(11)	6114.8(12)	6844(2)
Crystal size (mm)	0.32 × 0.12 × 0.03	0.22 × 0.16 × 0.09	0.30 × 0.15 × 0.05
Z	4	8	8
Density $_{calcd}$ (Mg/m^3)	1.159	1.207	1.166
Abs coeff (mm^{-1})	0.071	0.101	0.095
F (000)	1208	2360	2567
θ range (°)	1.355 to 30.947	1.529 to 30.537	1.47 to 30.78
Data collected (*hkl*)	±14, ±43, –15 to 8	–39 to 40, ±18, -25 to 17	–28 to 42, –16 to 17, –29 to 28
Reflns collected/unique	15858/4310	29891/9313	33844/10581
R(int)	0.0764	0.0551	0.1210
Max. and min. transmn	0.7461, 0.5575	0.7461, 0.6927	0.9953, 0.9722
Data/restrains/para	4310 / 1 / 196	9313 / 0 / 378	10581 / 0 / 408
Goodness-of-fit on F^2	1.020	1.015	0.965
Final R_1, wR_2 [I > 2σ(I)]	0.0521, 0.1235	0.0515, 0.1324	0.0717, 0.1589
R_1, wR_2 (all data)	0.0706, 0.1350	0.0911, 0.1561	0.1712, 0.2116
$\Delta\rho_{max}$, $_{min}$/e $Å^{-3}$	0.271, –0.205	0.466, –0.339	0.426, –0.424

Table S2. Crystallographic data for complexes **3**, **6** and **8**

	3	**6**	**8**
Empirical formula	$C_{65}H_{65}AlN_2O_2$	$C_{77}H_{83}Al_2N_2O_2$	$C_{41}H_{49}AlN_2O_3$
Formula weight	933.17	1122.41	644.80
Temp (K)	140(2)	140(2)	140(2)
Wavelength (Å)	0.71073	0.71073	0.71073
Crystal system	Triclinic	Triclinic	Monoclinic
Space group	P -1	P -1	C 2/c
a (Å)	15.337(3)	11.4917(18)	29.753(3)
b (Å)	18.328(3)	17.564(3)	12.0799(10)
c (Å)	22.205(4)	18.529(3)	21.3364(19)
α (°)	112.830(3)	106.220(3)	90
β (°)	90.449(3)	107.539(3)	104.425(2)
γ (°)	110.283(3)	102.510(3)	90
Volume (Å^3)	5322.4(17)	3234.0(9)	7426.9(11)
Crystal size (mm)	0.220 × 0.160 × 0.100	0.36 × 0.26 × 0.15	0.200 × 0.080 × 0.060
Z	4	2	8
Density $_{calcd}$ (Mg/m^3)	1.165	1.153	1.153
Abs coeff (mm^{-1})	0.084	0.093	0.093
F (000)	1992	1202	2768
θ range (°)	1.009 to 27.661	1.24 to 26.00	1.828 to 30.629
Data collected (*hkl*)	–19 to 20, ±23, –23 to 28	–13 to 14, –21 to 20, ±22	±42, –12 to 17, ±30
Reflns collected/unique	43450/24571	23299/12653	37343/11416
R(int)	0.0799	0.0540	0.0952
Max. and min. transmn	0.7456, 0.6071	0.9862, 0.9674	0.7461, 0.6837
Data/restrains/para	24571 / 36 /1283	12653 / 1 / 294	11416 / 0 / 436
Goodness-of-fit on F^2	0.947	1.026	0.955
Final R_1, wR_2 [I > 2σ(I)]	0.0710, 0.1760	0.0781, 0.2039	0.0572, 0.1106
R_1, wR_2 (all data)	0.1660, 0.2407	0.1331, 0.2653	0.1505, 0.1437
$\Delta\rho_{max}$, $_{min}$/e Å^{-3}	0.668, –0.347	1.273, –0.442	0.308, –0.322

Table S3. Crystallographic data for complexes **9**, **10** and **11**

	9	**10**	**11**
Empirical formula	C_{45} H_{49} Al N_2 O_3	C_{43} H_{51} Al N_2 O_5	C_{42} H_{48} Al N_2 O_5
Formula weight	692.84	702.83	687.80
Temp (K)	140(2)	143(2)	130
Wavelength (Å)	0.71073	0.71073	0.71073
Crystal system	Orthorhombic	Triclinic	Triclinic
Space group	P 21 21 21	P -1	P -1
a (Å)	12.2232(13)	14.0490(14)	13.950(3)
b (Å)	15.5668(16)	16.3570(17)	16.296(3)
c (Å)	20.211(2)	21.740(2)	21.630(4)
α (°)	90	91.197(2)	91.070(3)
β (°)	90	94.859(2)	95.849(3)
γ (°)	90	113.992(2)	114.041(3)
Volume ($Å^3$)	3845.6(7)	4539.4(8)	4457.2(14)
Crystal size (mm)	0.200 × 0.160 × 0.080	0.250 × 0.150 × 0.030	0.25 × 0.2 × 0.15
Z	4	4	4
Density $_{calcd}$ (Mg/m^3)	1.197	1.028	1.025
Abs coeff (mm^{-1})	0.095	0.084	0.085
F (000)	1480	1504	1468
θ range (°)	1.651 to 30.530	0.942 to 30.754	0.948 to 26.000
Data collected (*hkl*)	±42, ±22, -24 to 28	-20 to 13, ±23, ±31	-19 to20, -18 to 23, ±30
Reflns collected/unique	39163/11764	46825/27926	44848/17512
R(int)	0.0981	0.0680	0.0590
Max. and min. transmn	0.7461, 0.6827	0.7461, 0.6275	0.7461, 0.5752
Data/restrains/para	11764 / 0 / 470	27926 / 0 / 945	17512 / 53 / 945
Goodness-of-fit on F^2	0.993	0.861	1.105
Final R_1, wR_2 [I > 2σ(I)]	0.0614, 0.1092	0.0710, 0.1533	0.0787, 0.2097
R_1 , wR_2 (all data)	0.1248, 0.1319	0.1835, 0.1793	0.1131, 0.2237
$\Delta\rho_{max,\ min}$/e $Å^{-3}$	0.238, –0.316	0.302, –0.319	0.603, –0.685

Table S4. Selected bond distances (Å) and angles (◦) for complexes **10** and **11**

		10	
Al1–O1	1.847(2)	Al1–O2	1.8291(19)
Al1–O3	1.817(2)	Al1–O4	2.0296(19)
Al1–N1	2.007(2)	Al1–N2	2.073(2)
O1–Al1–O2	90.48(9)	O1–Al1–O3	97.18(9)
O1–Al1–O4	89.06(8)	O2–Al1–O3	168.09(9)
O2–Al1–O4	88.70(8)	O3–Al1–O4	82.35(8)
O1–Al1–N1	89.03(9)	O1–Al1–N2	175.38(10)
O2–Al1–N1	94.90(9)	O2–Al1–N2	85.19(9)
O3–Al1–N1	94.33(9)	O3–Al1–N2	87.35(9)
O4–Al1–N1	175.93(9)	O4–Al1–N2	92.45(8)
N1–Al1–N2	89.73(9)		
Al2–O6	1.8188(19)	Al2–O7	1.8174(19)
Al2–O8	1.8056(19)	Al2–O9	2.023(2)
Al2–N3	2.090(2)	Al2–N4	2.045(2)
O6–Al2–O7,	96.35(10)	O6–Al2–O8	97.02(11)
O6–Al2–O9	172.33(10)	O7–Al2–O8	96.46(10)
O7–Al2–O9	91.26(9)	O8–Al2–O9	83.04(10)
O6–Al2–N3	87.00(10)	O6–Al2–N4	94.74(11)
O7–Al2–N3	171.18(12)	O7–Al2–N4	86.90(10)
O8–Al2–N3	91.21(11)	O8–Al2–N4	167.32(11)
O9–Al2–N3	85.34(9)	O9–Al2–N4	84.67(10)
N3–Al2–N4	84.68(11)		
		11	
Al1–O1	1.822(2)	Al1–O2	1.849(2)
Al1–O3	1.812(2)	Al1–O4	2.039(2)
Al1–N1	2.063(3)	Al1–N2	2.005(3)
O1–Al1–O2	91.47(10)	O1–Al1–O3	169.66(12)
O1–Al1–O4	89.07(10)	O2–Al1–O3	95.16(10)
O2–Al1–O4	89.62(10)	O3–Al1–O4	83.06(10)
O1–Al1–N1	85.33(10)	O1–Al1–N2	93.98(11)
O2–Al1–N1	176.79(11)	O2–Al1–N2	90.11(10)
O3–Al1–N1	87.99(10)	O3–Al1–N2	93.93(11)
O4–Al1–N1	90.16(10)	O4–Al1–N2	176.94(10)
N1–Al1–N2	90.28(11)		
Al2–O6	1.805(2)	Al2–O7	1.828(2)
Al2–O8	1.808(2)	Al2–O9	2.038(2)

Al2–N3	2.079(3)	Al2–N4	2.059(3)
O6–Al2–O7	96.27(9)	O6–Al2–O8	96.88(9)
O6–Al2–O9	171.56(9)	O7–Al2–O8	96.54(9)
O7–Al2–O9	92.13(8)	O8–Al2–O9	82.98(8)
O6–Al2–N3	86.79(9)	O6–Al2–N4	94.56(9)
O7–Al2–N3	170.63(9)	O7–Al2–N4	86.76(9)
O8–Al2–N3	91.87(9)	O8–Al2–N4	167.66(10)
O9–Al2–N3	84.78(9)	O9–Al2–N4	85.02(9)
N3–Al2–N4	84.17(9)		

3. NMR spectra of complexes 1–11

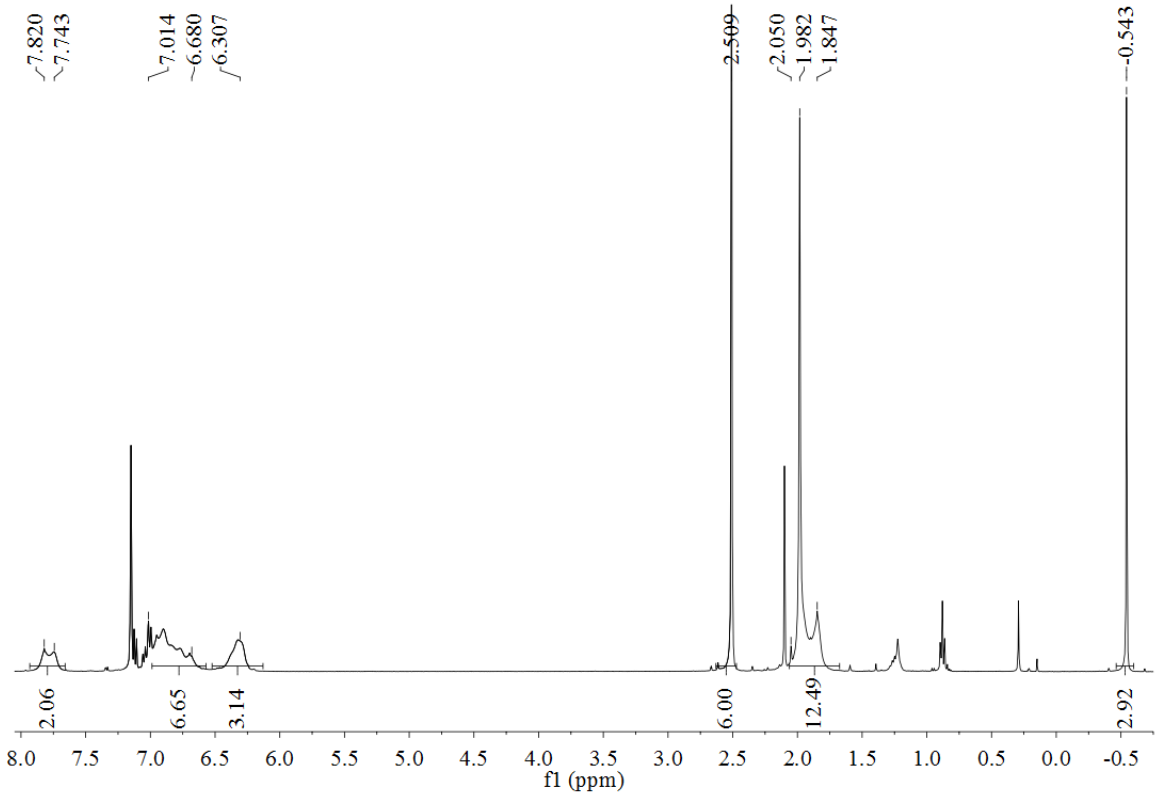

Figure S5. ^{1}H NMR spectrum of complex **1** (400 MHz, C_6D_6, 25 ℃).

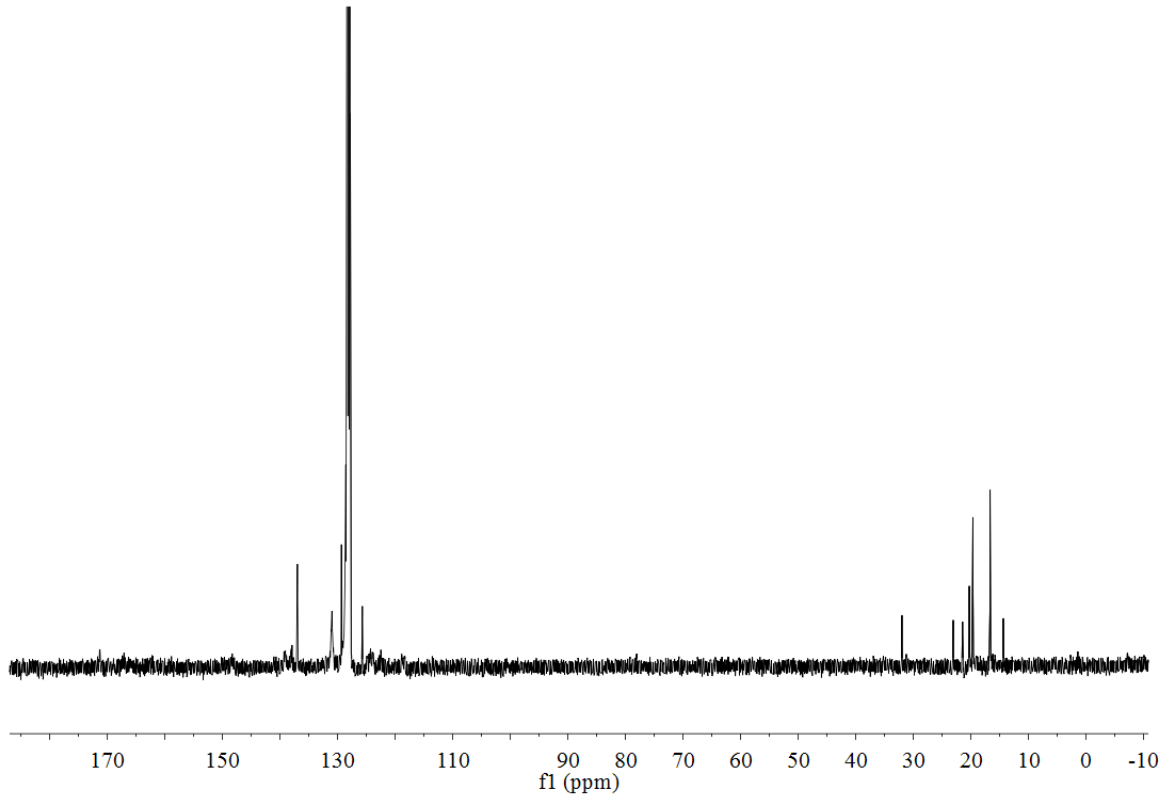

Figure S6. ^{13}C NMR spectrum of complex **1** (100 MHz, C_6D_6, 25 ℃).

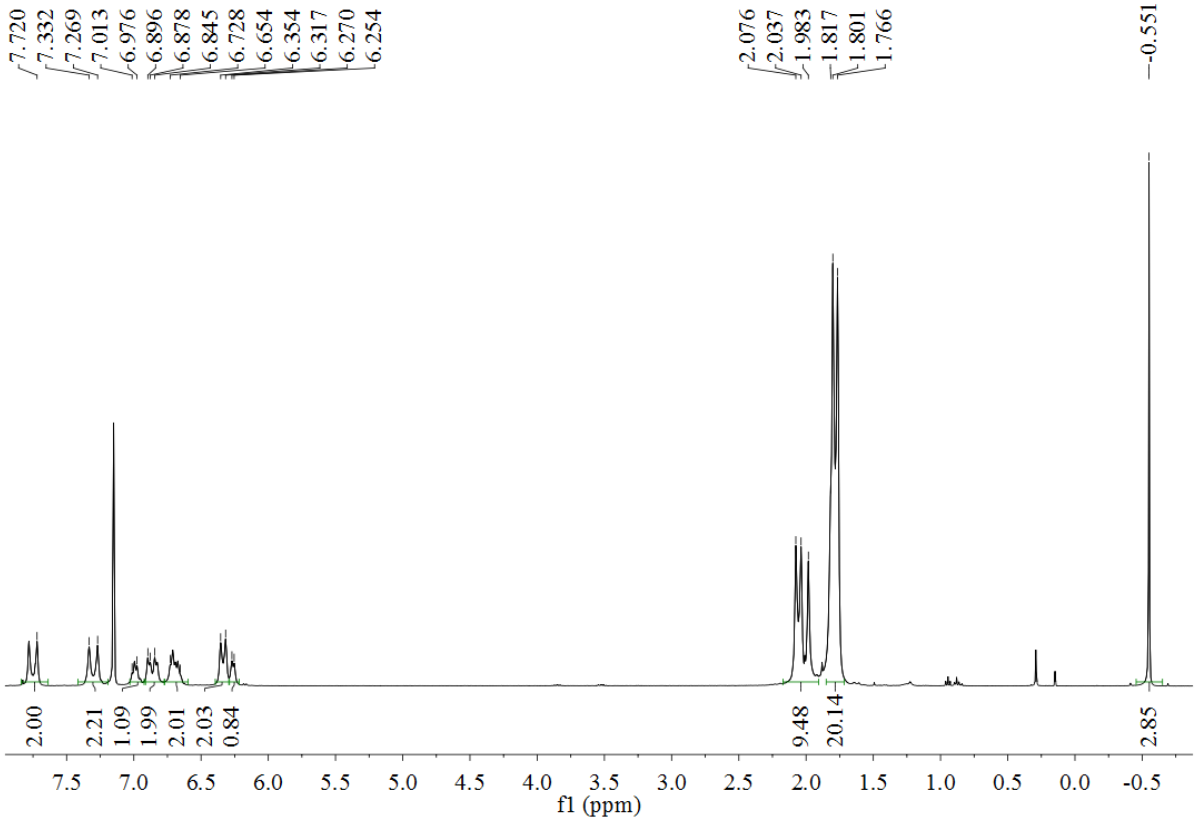

Figure S7. ^{1}H NMR spectrum of complex **2** (400 MHz, C_6D_6, 25 ℃).

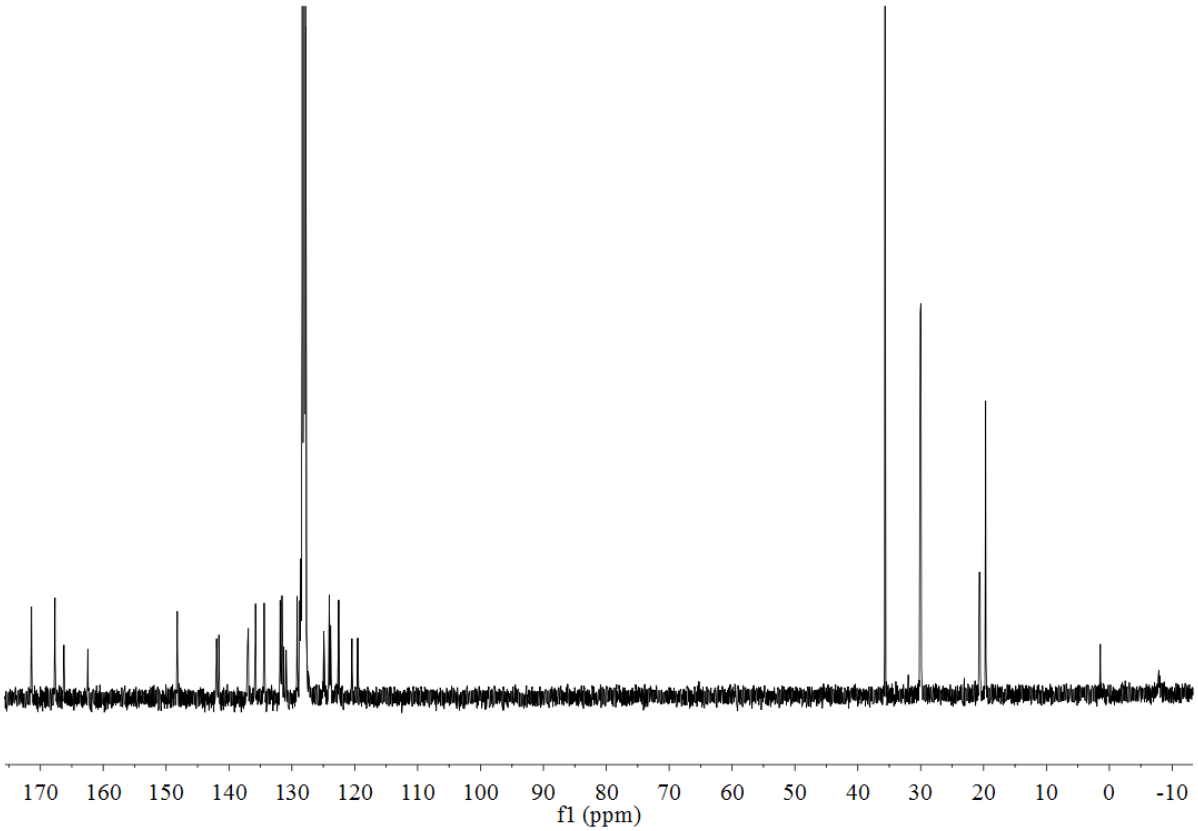

Figure S8. ^{13}C NMR spectrum of complex **2** (100 MHz, C_6D_6, 25 ℃).

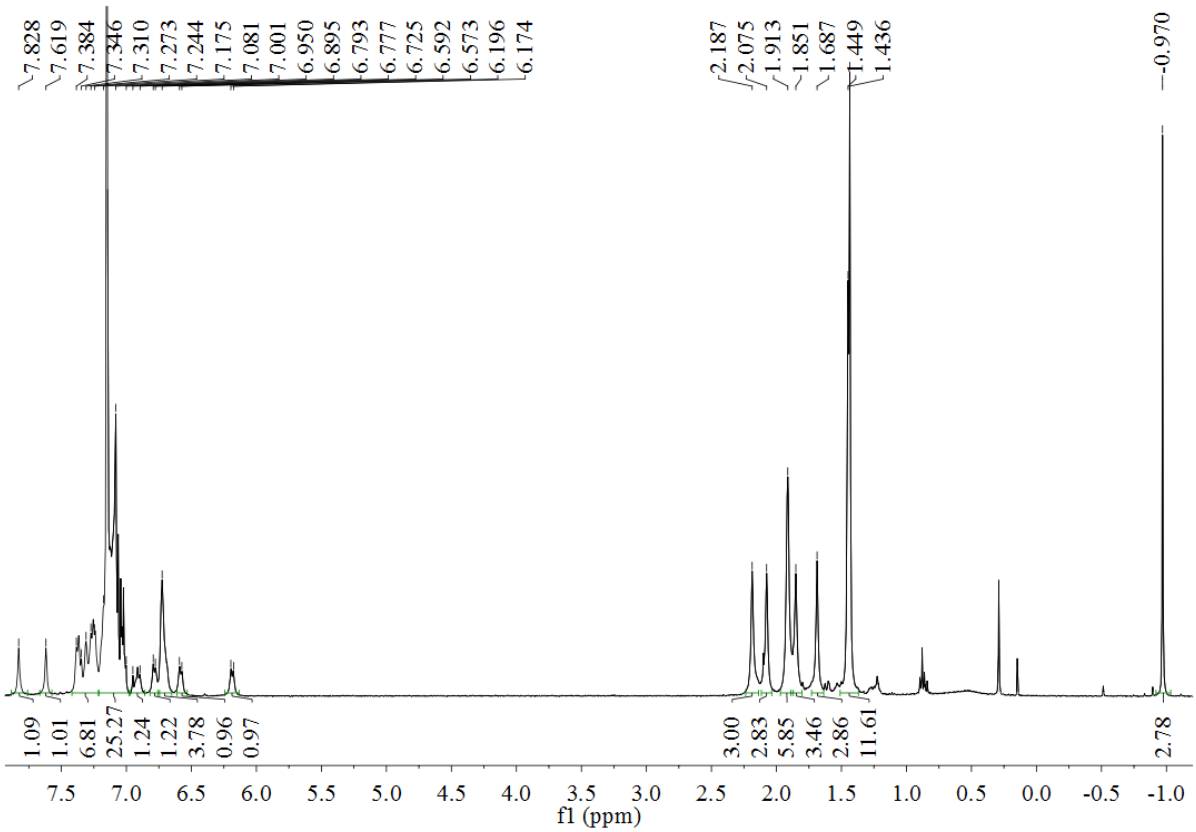

Figure S9. ^{1}H NMR spectrum of complex **3** (400 MHz, C_6D_6, 25 ℃).

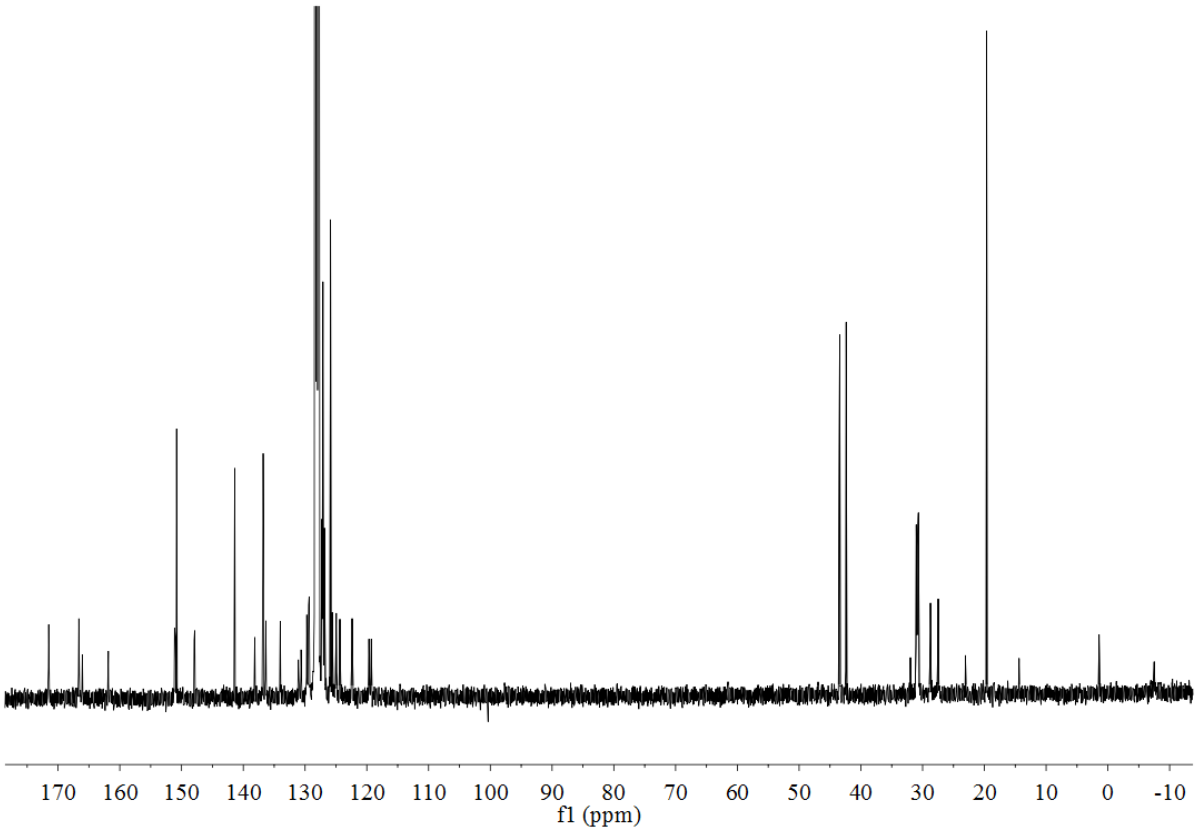

Figure S10. ^{13}C NMR spectrum of complex **3** (100 MHz, C_6D_6, 25 ℃).

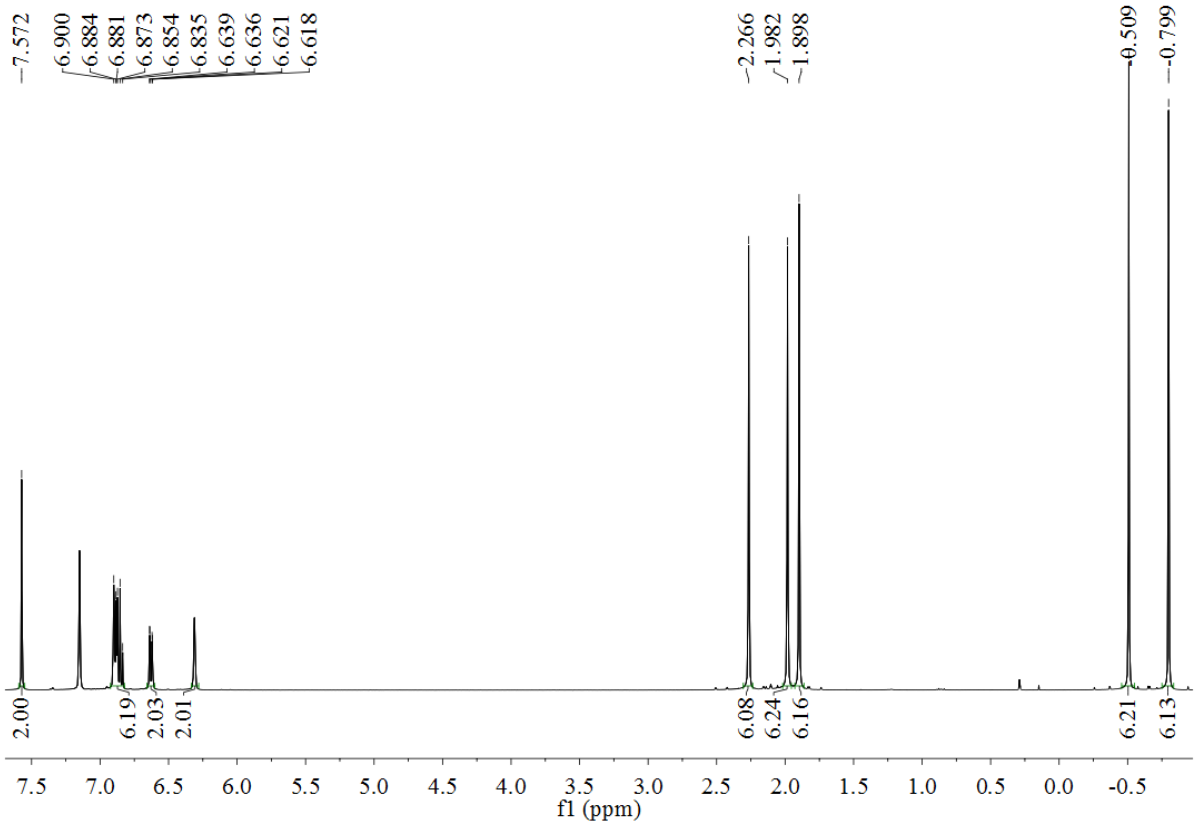

Figure S11. ^{1}H NMR spectrum of complex **4** (400 MHz, C_6D_6, 25 ℃).

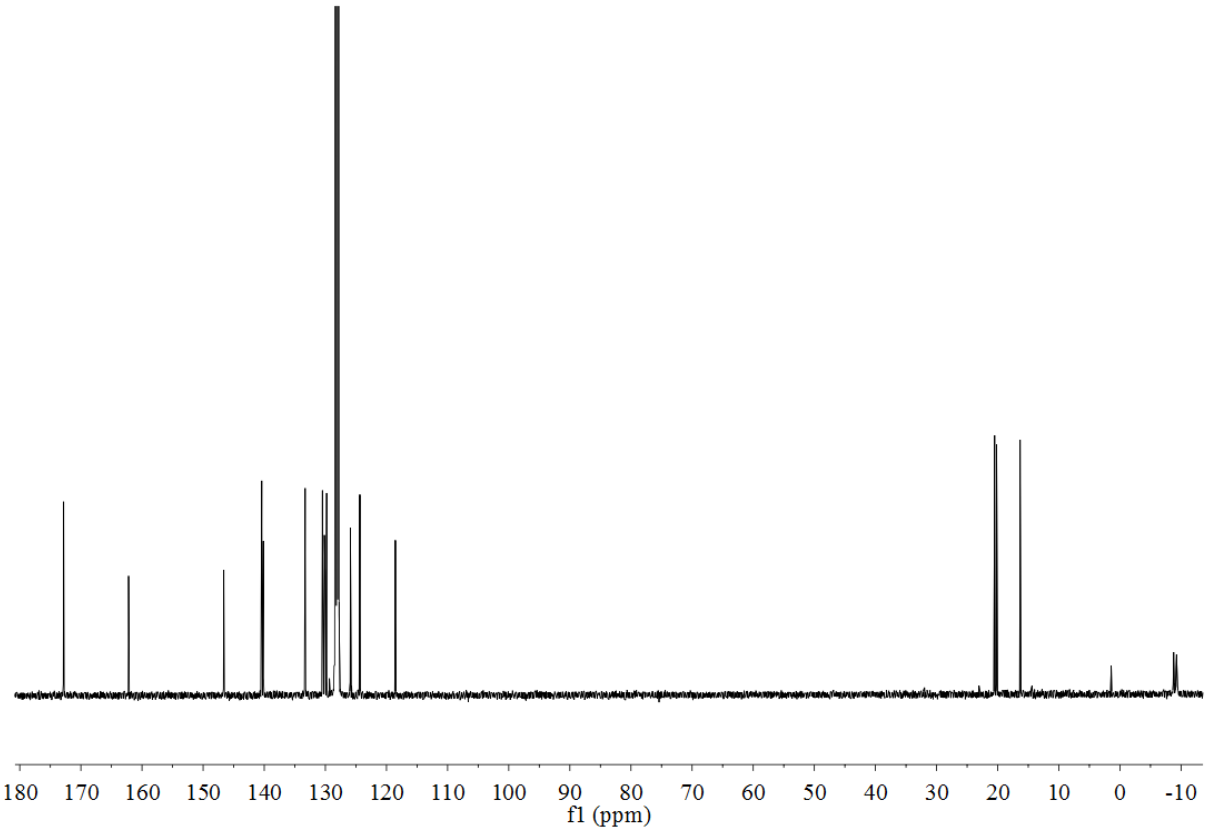

Figure S12. ^{13}C NMR spectrum of complex **4** (100 MHz, C_6D_6, 25 ℃).

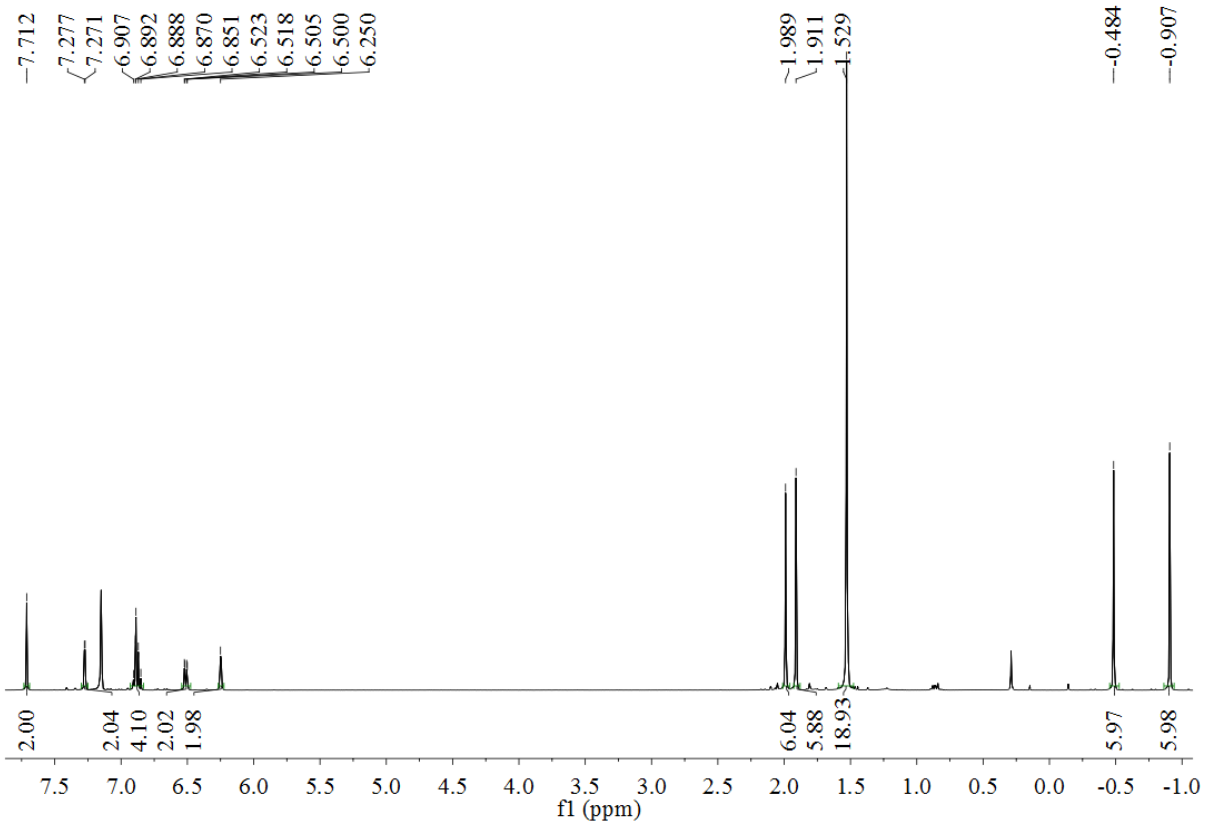

Figure S13. ^{1}H NMR spectrum of complex **5** (400 MHz, C_6D_6, 25 ℃).

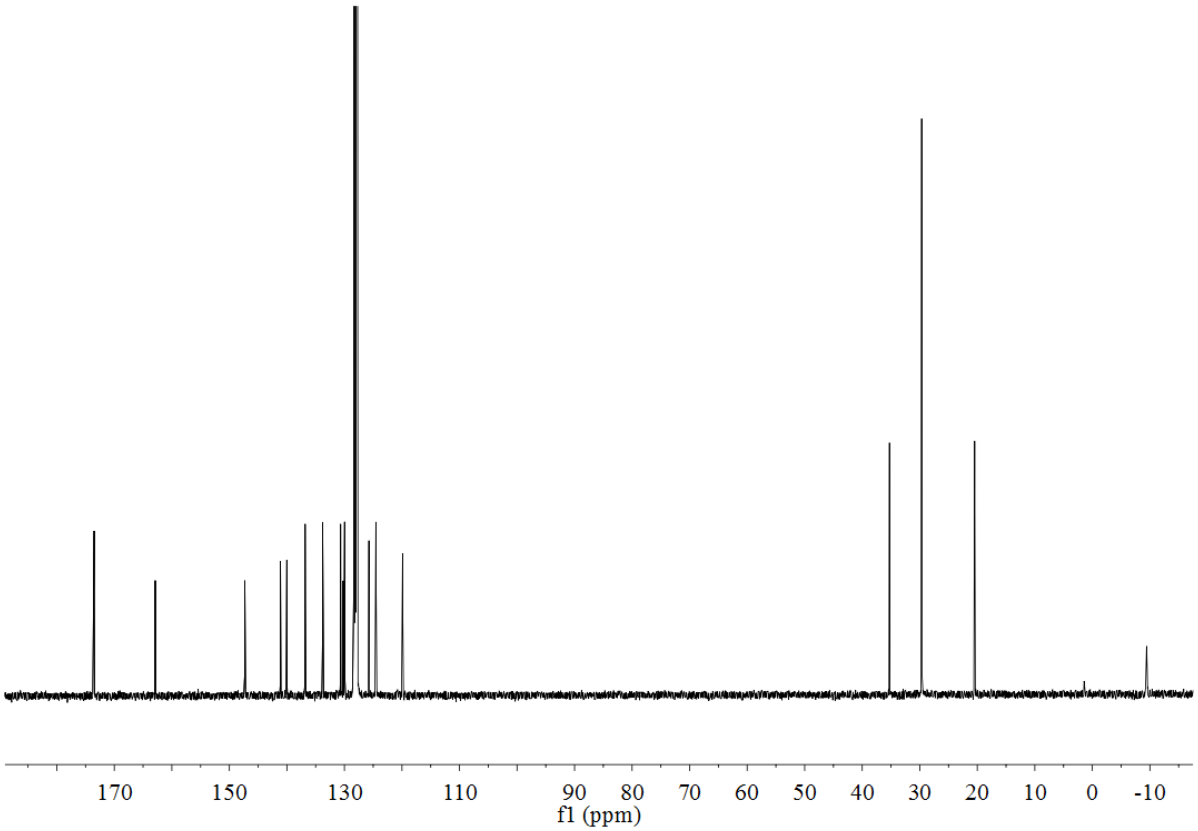

Figure S14. ^{13}C NMR spectrum of complex **5** (100 MHz, C_6D_6, 25 ℃).

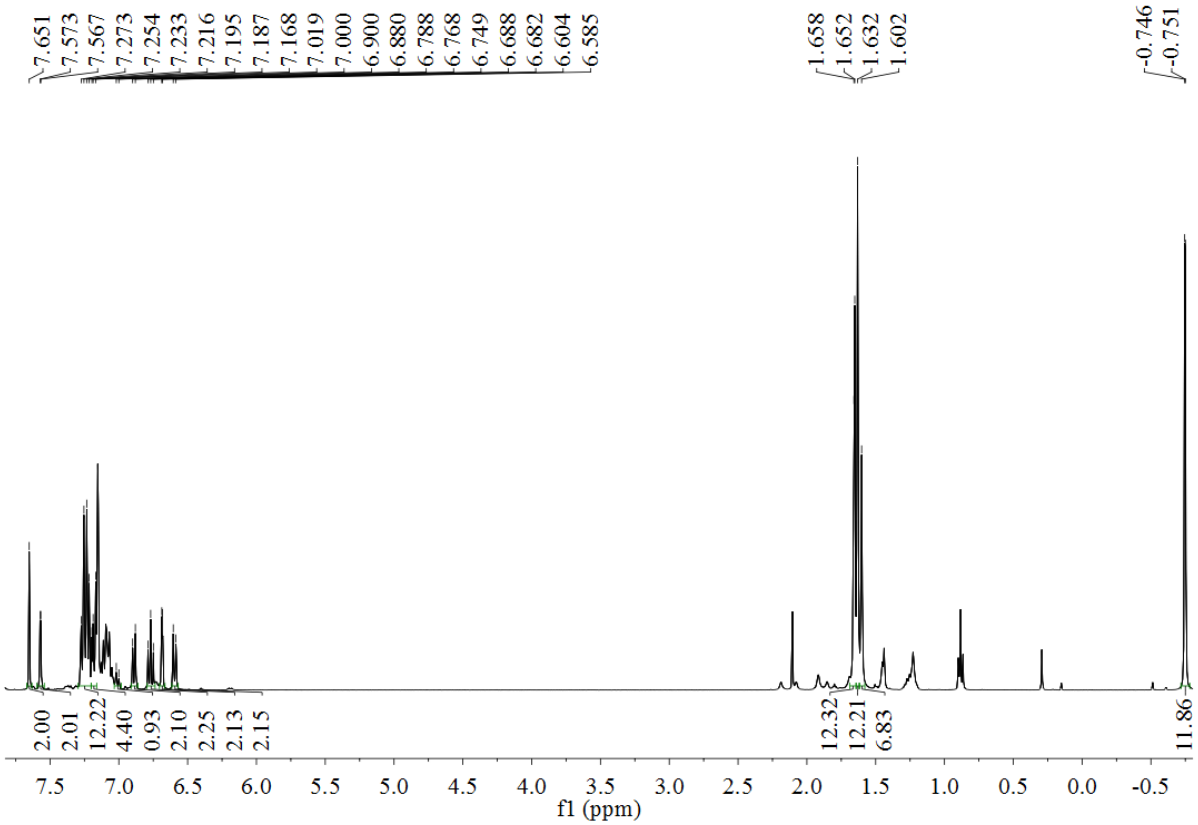

Figure S15. ^{1}H NMR spectrum of complex **6** (400 MHz, C_6D_6, 25 ℃).

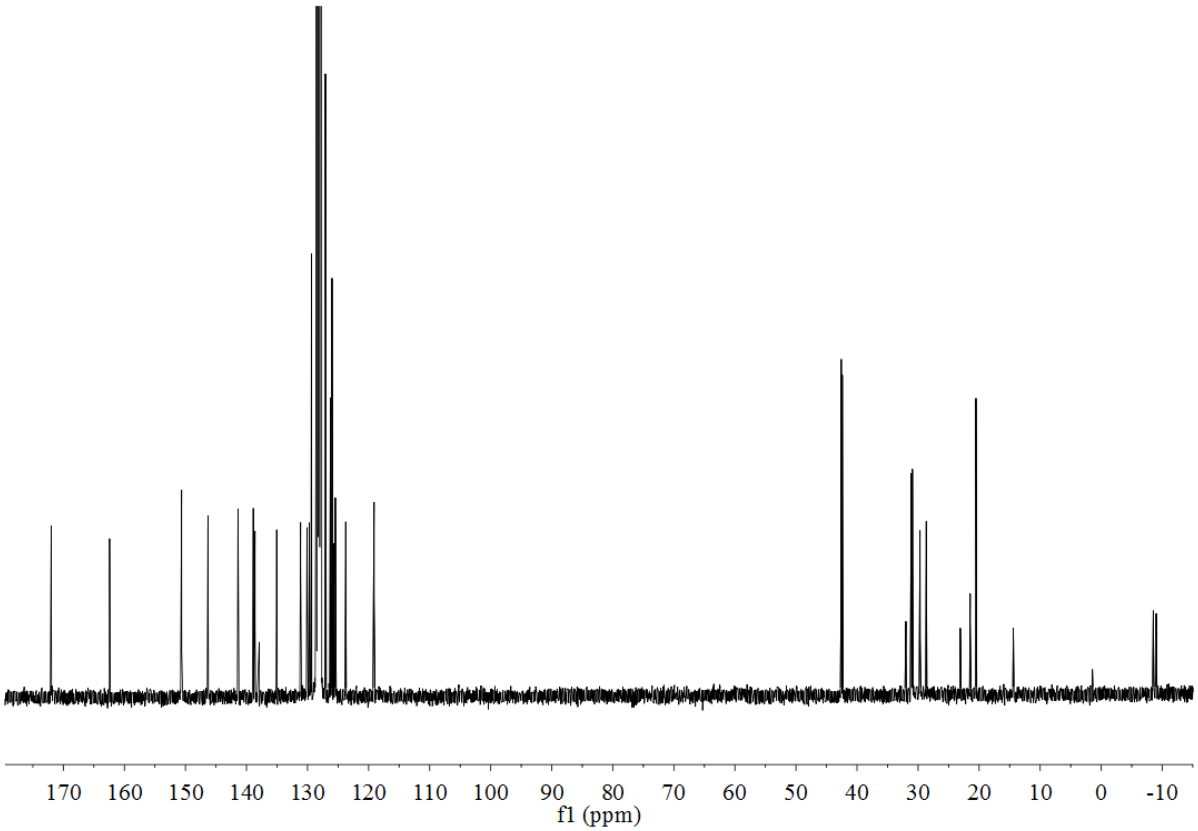

Figure S16. ^{13}C NMR spectrum of complex **6** (100 MHz, C_6D_6, 25 ℃).

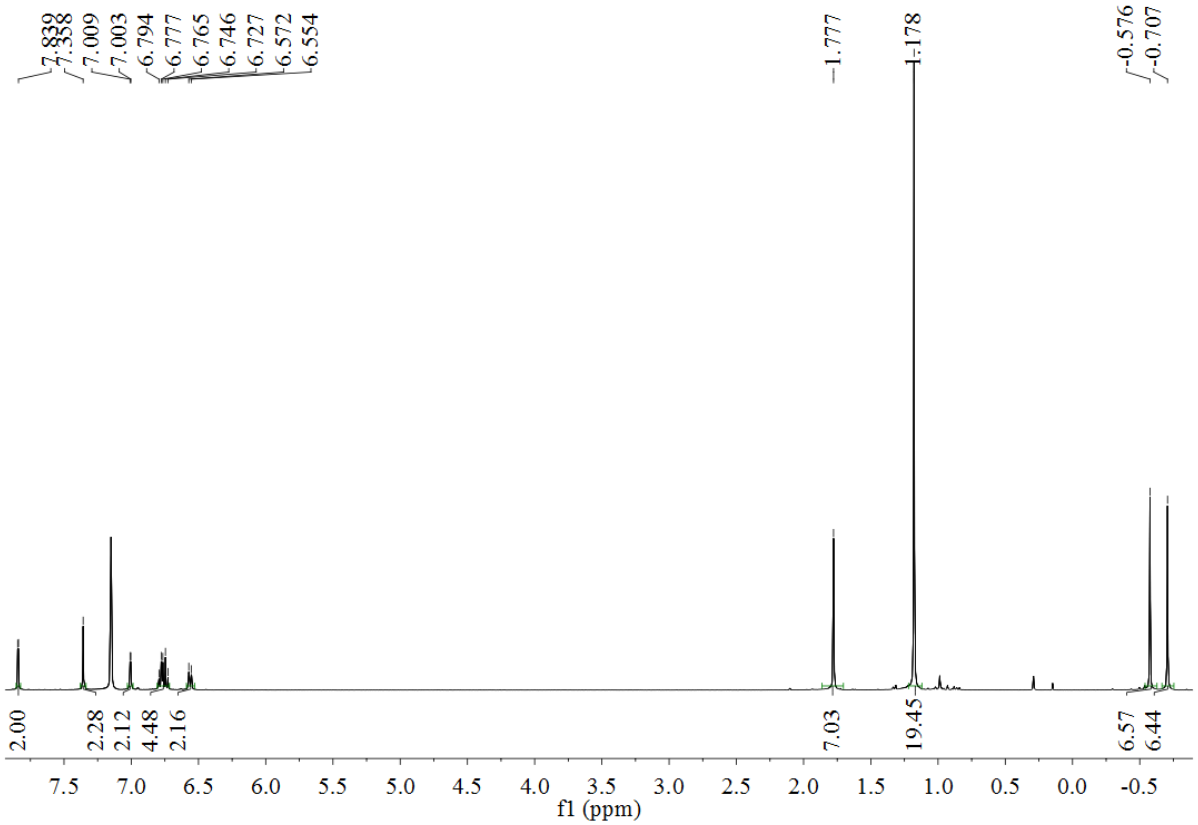

Figure S17. ^{1}H NMR spectrum of complex **7** (400 MHz, C_6D_6, 25 ℃).

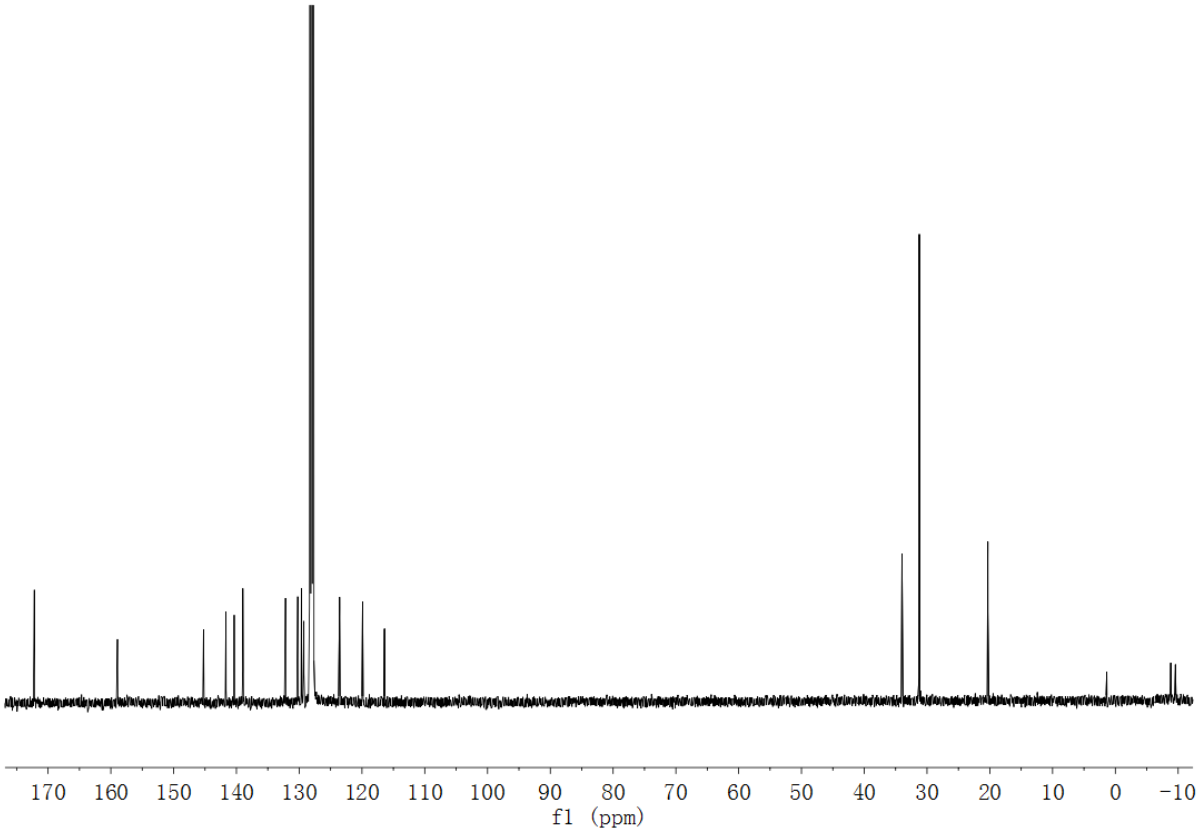

Figure S18. ^{13}C NMR spectrum of complex **7** (100 MHz, C_6D_6, 25 ℃).

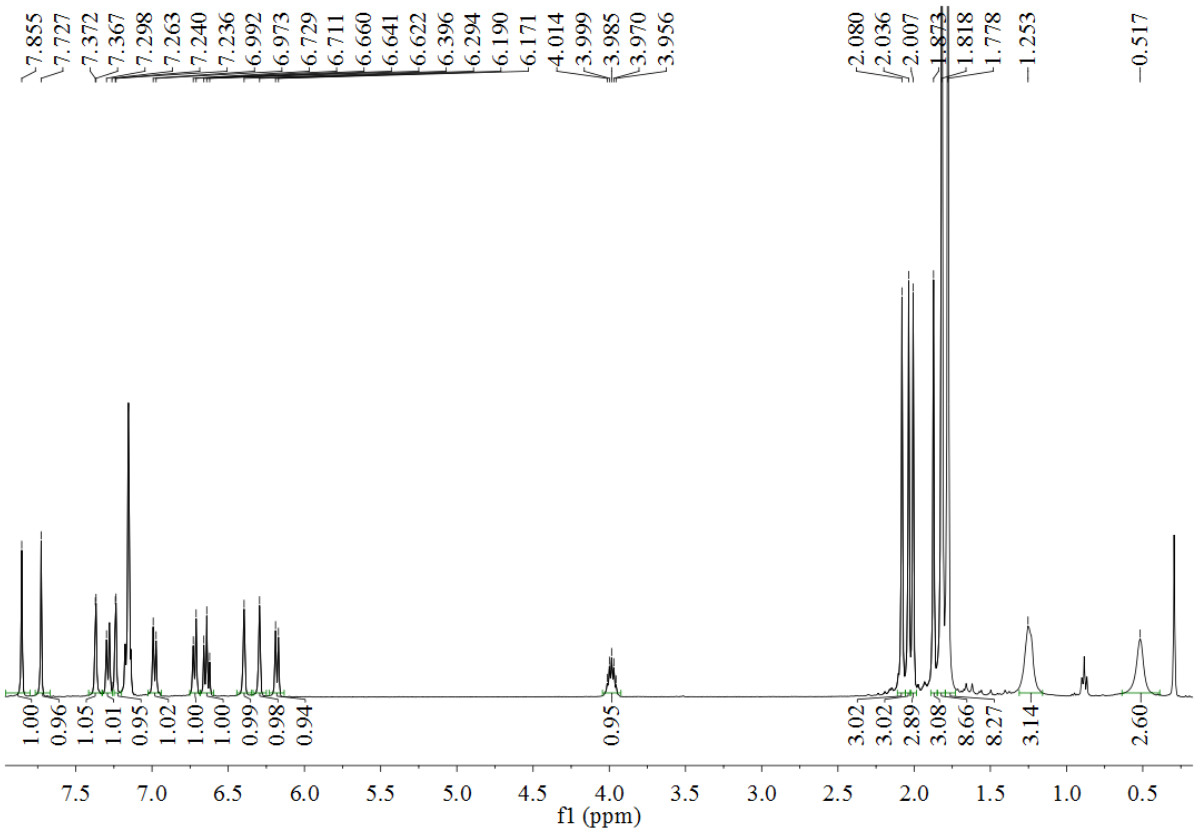

Figure S19. ^{1}H NMR spectrum of complex **8** (400 MHz, C_6D_6, 25 ℃).

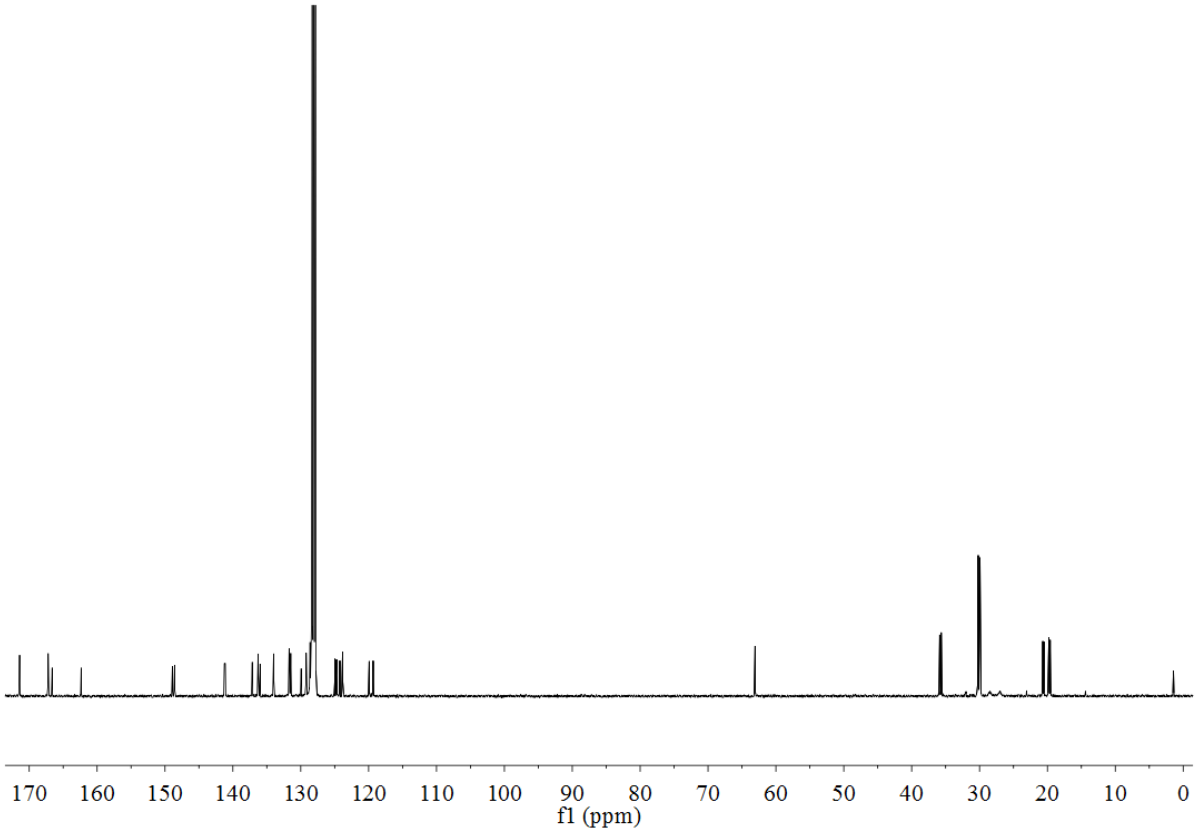

Figure S20. ^{13}C NMR spectrum of complex **8** (100 MHz, C_6D_6, 25 ℃).

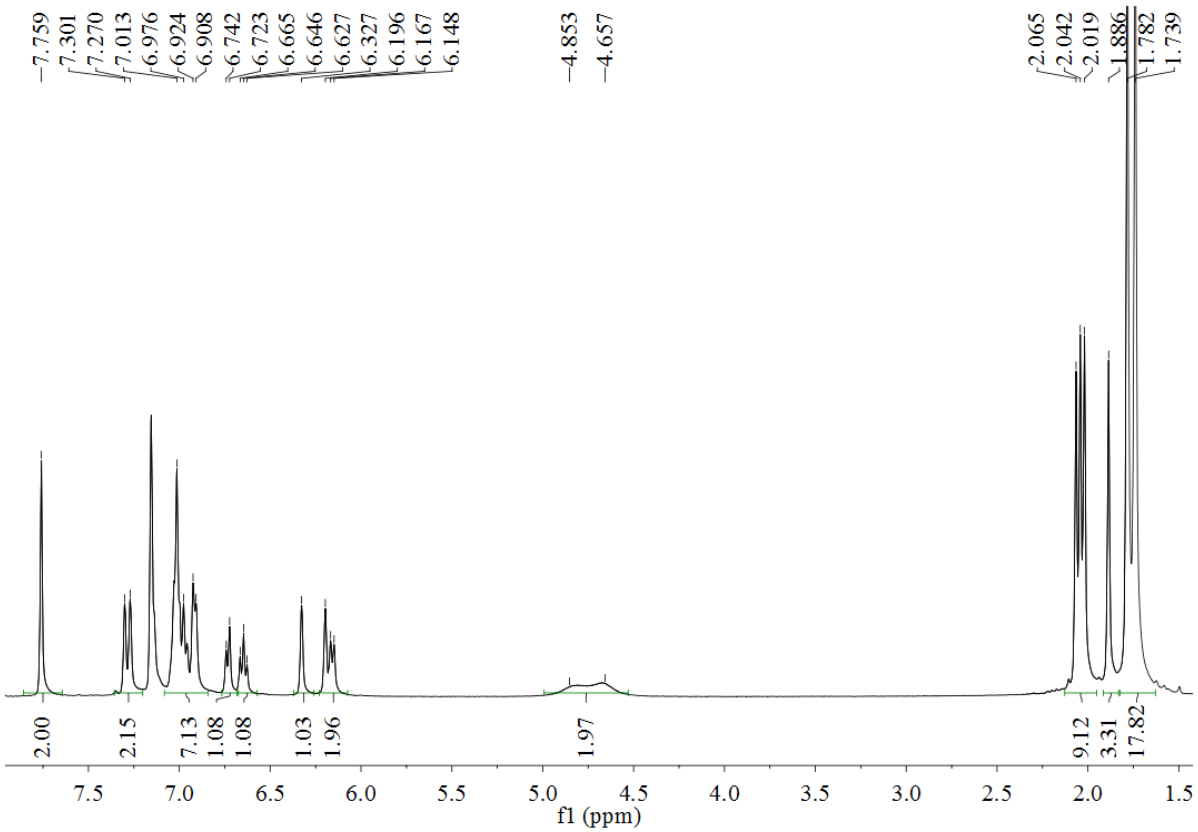

Figure S21. ^{1}H NMR spectrum of complex **9** (400 MHz, C_6D_6, 25 ℃).

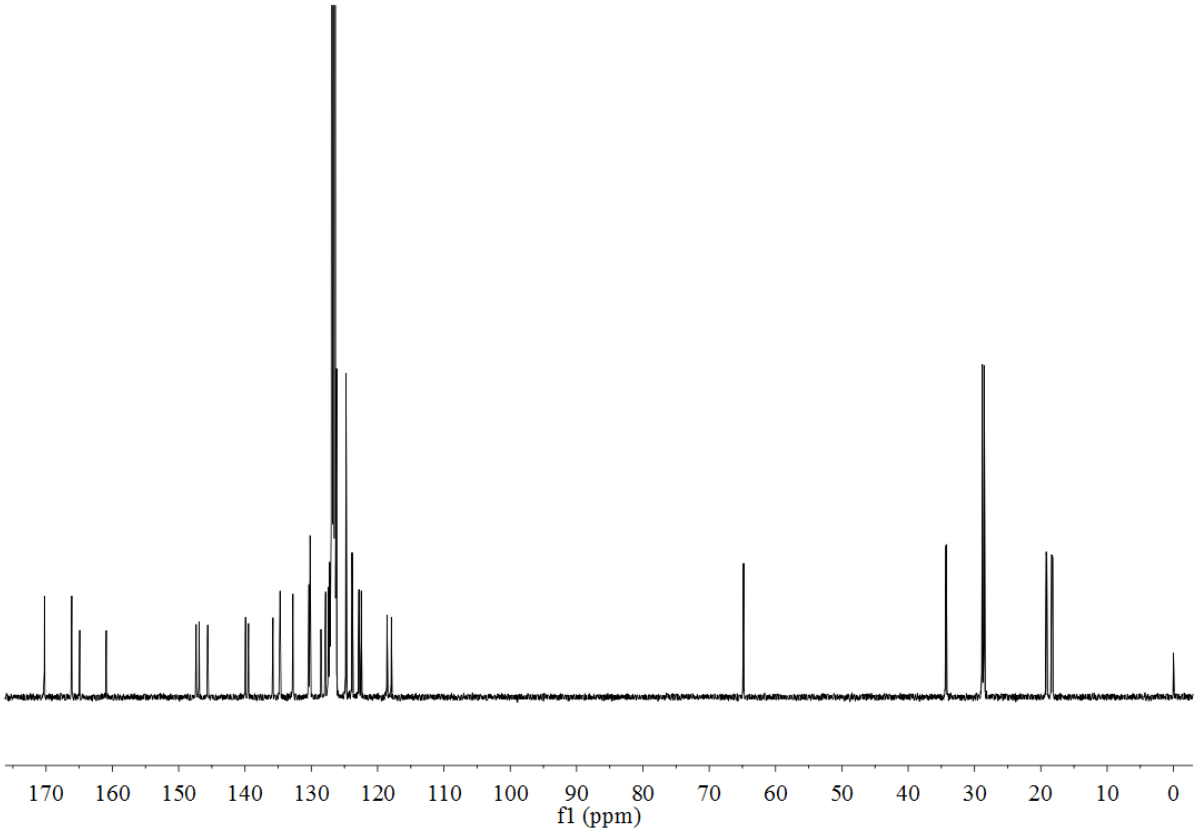

Figure S22. ^{13}C NMR spectrum of complex **9** (100 MHz, C_6D_6, 25 ℃).

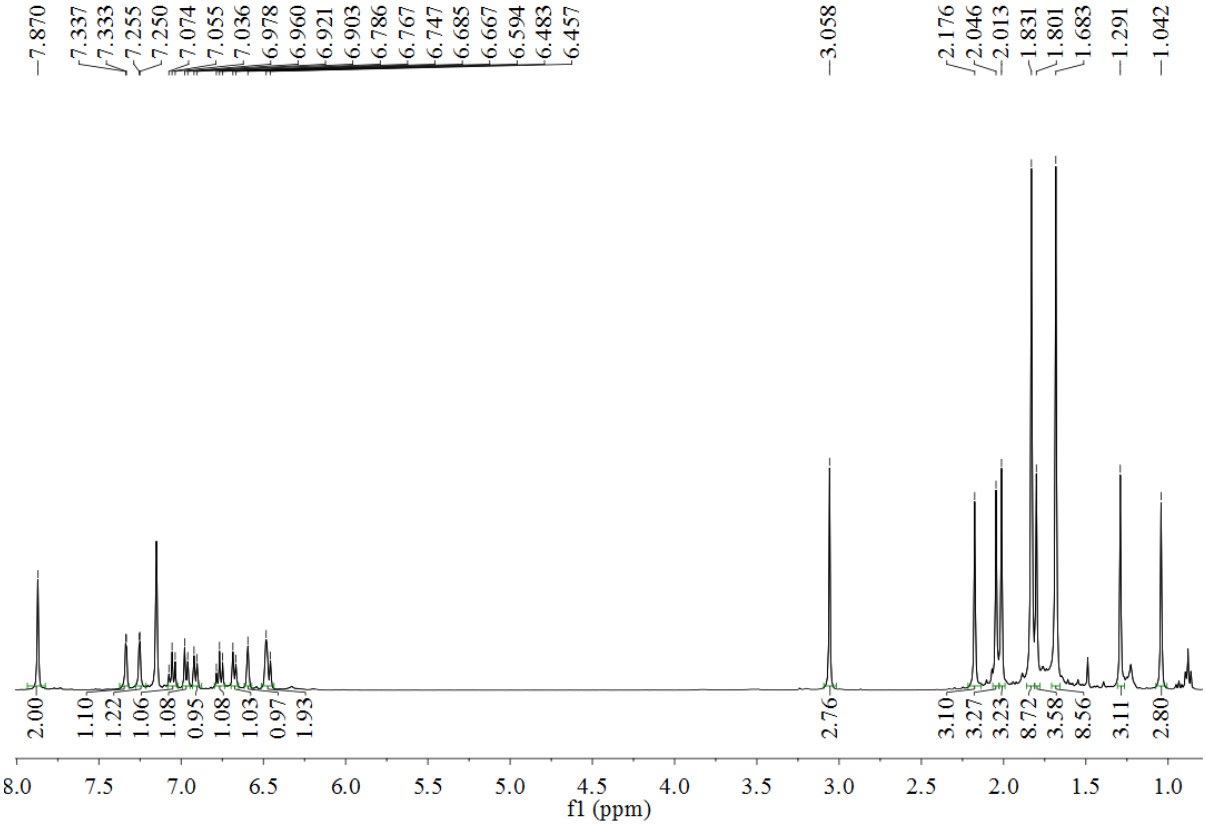

Figure S23. ^{1}H NMR spectrum of complex **10** (400 MHz, C_6D_6, 25 ℃).

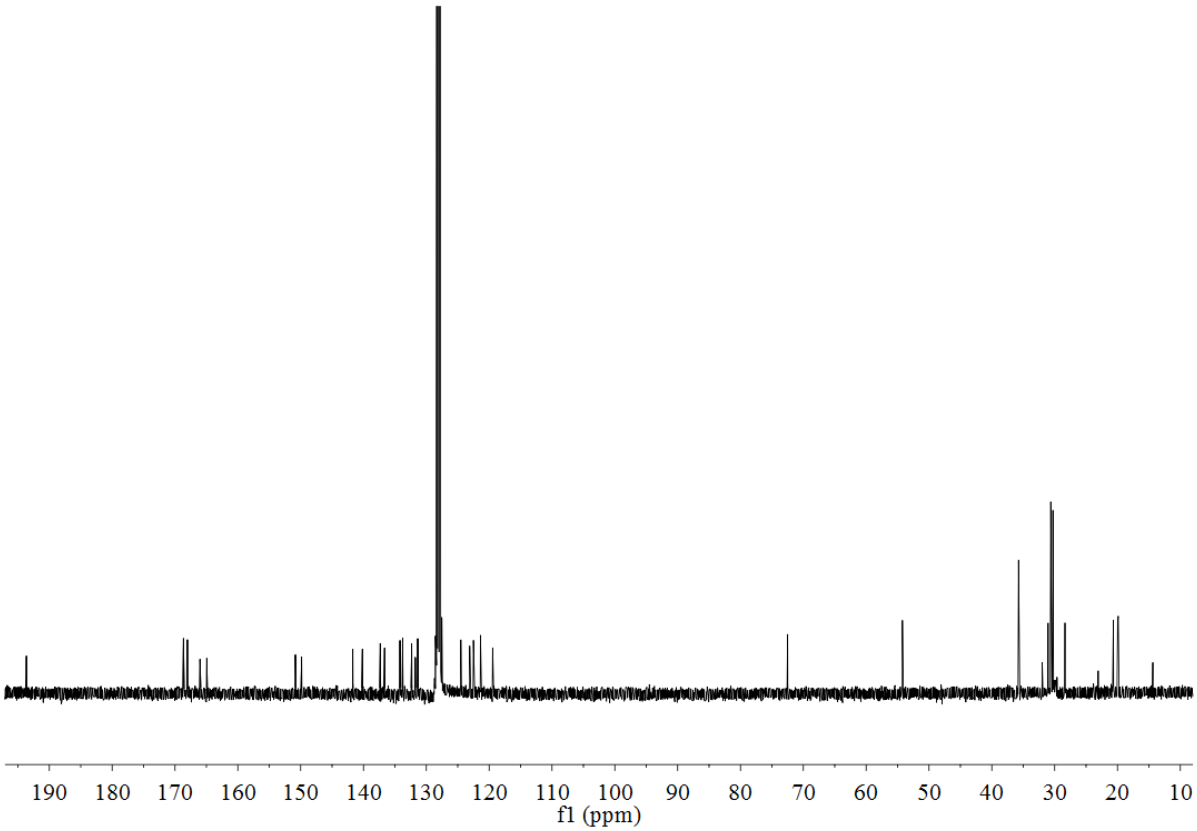

Figure S24. ^{13}C NMR spectrum of complex **10** (100 MHz, C_6D_6, 25 ℃).

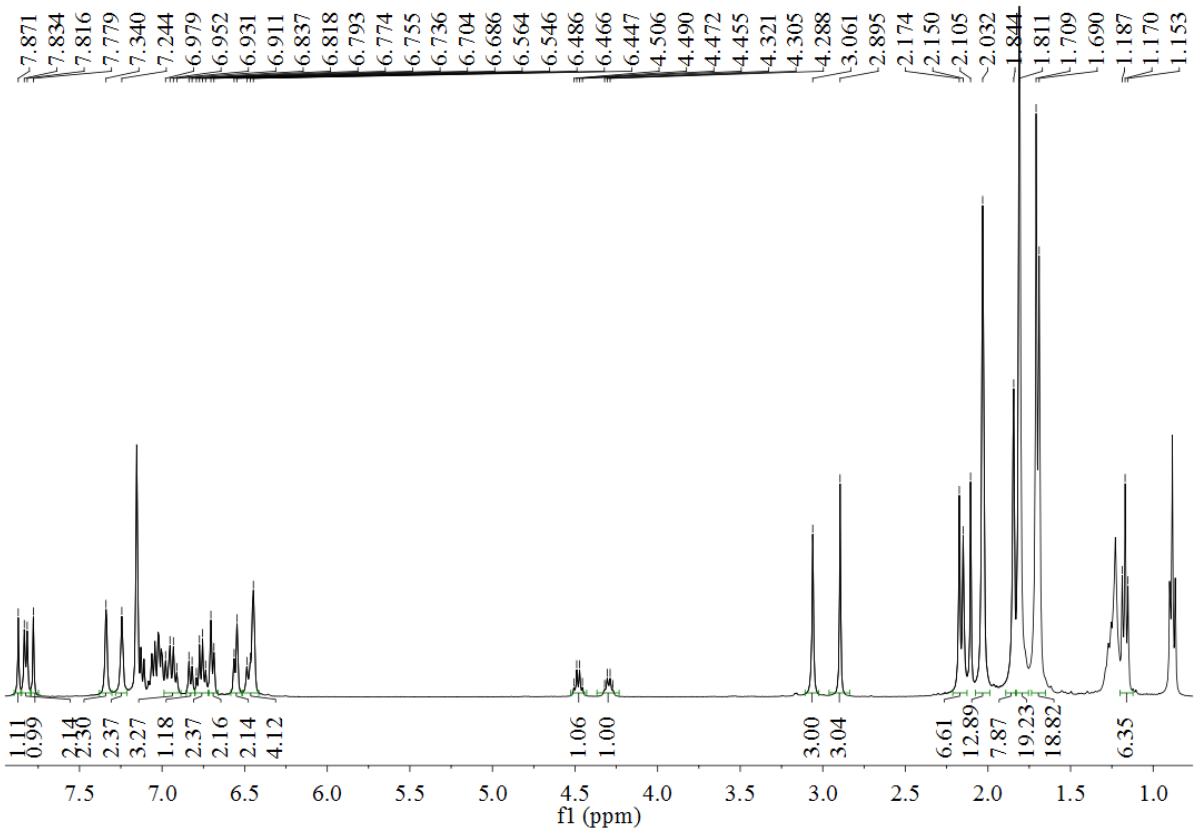

Figure S25. ^{1}H NMR spectrum of complex **11** (400 MHz, C_6D_6, 25 ℃).

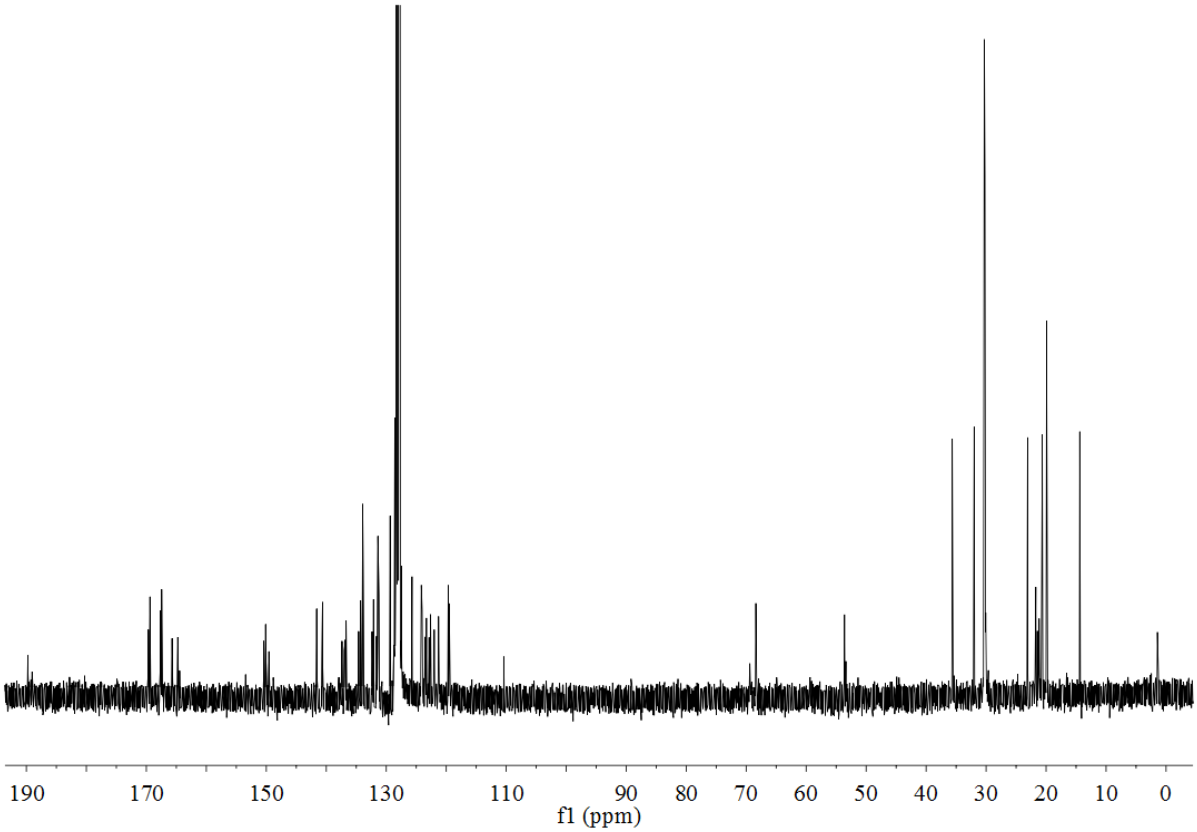

Figure S26. ^{13}C NMR spectrum of complex **11** (100 MHz, C_6D_6, 25 ℃).

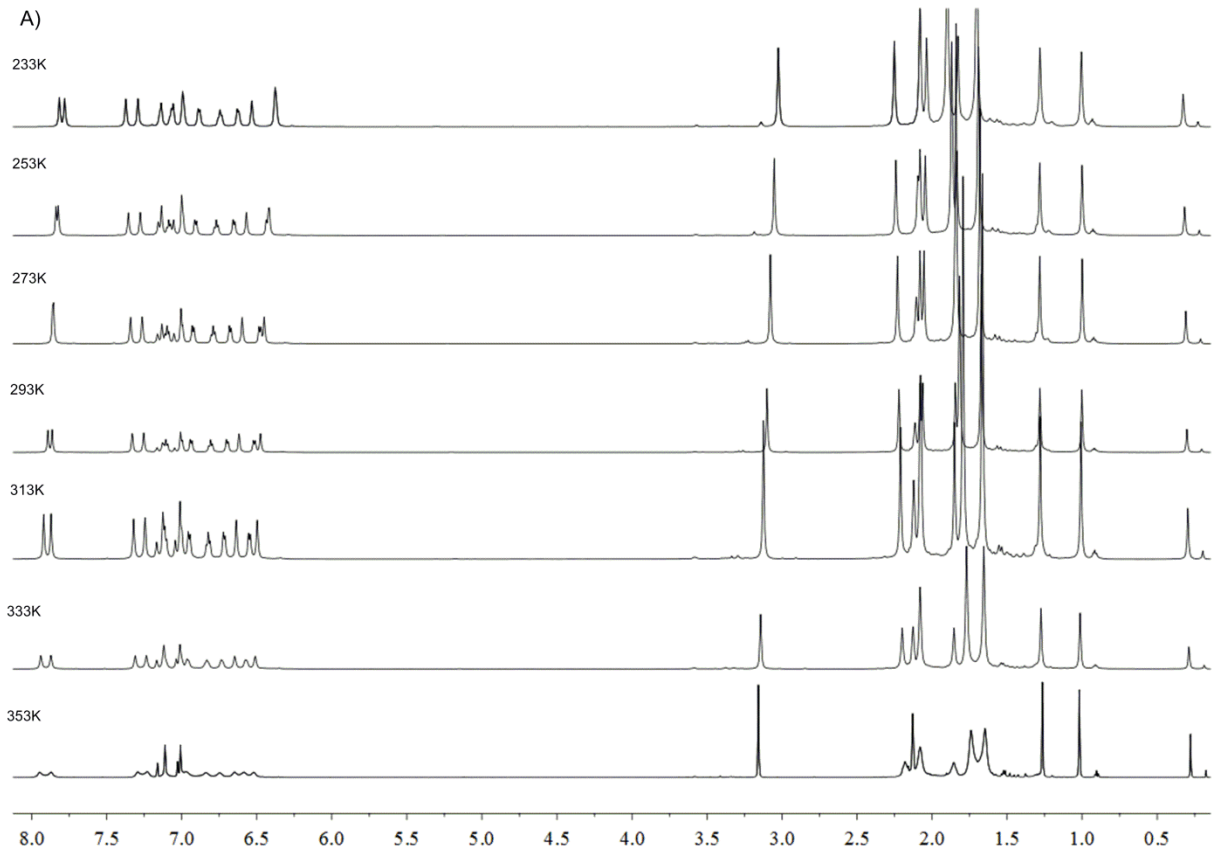
A)
233K
253K
273K
293K
313K
333K
353K
8.0
7.5
7.0
6.5
6.0
5.5
5.0
4.5
4.0
3.5
3.0
2.5
2.0
1.5
1.0
0.5

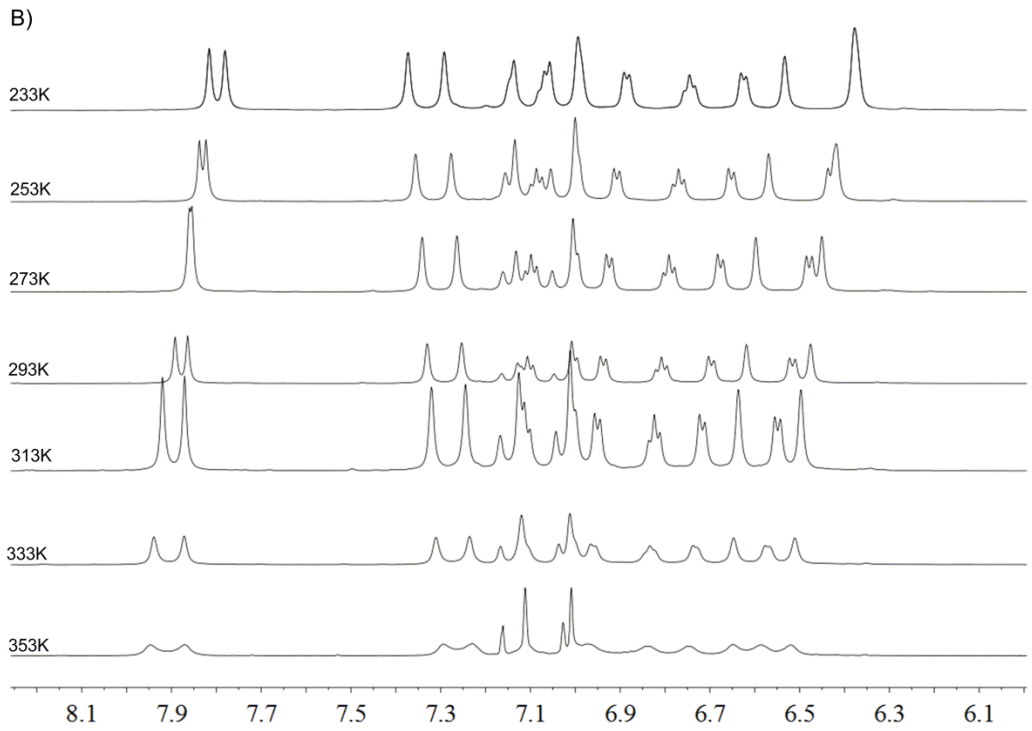
B)
233K
253K
273K
293K
313K
333K
353K
8.1
7.9
7.7
7.5
7.3
7.1
6.9
6.7
6.5
6.3
6.1

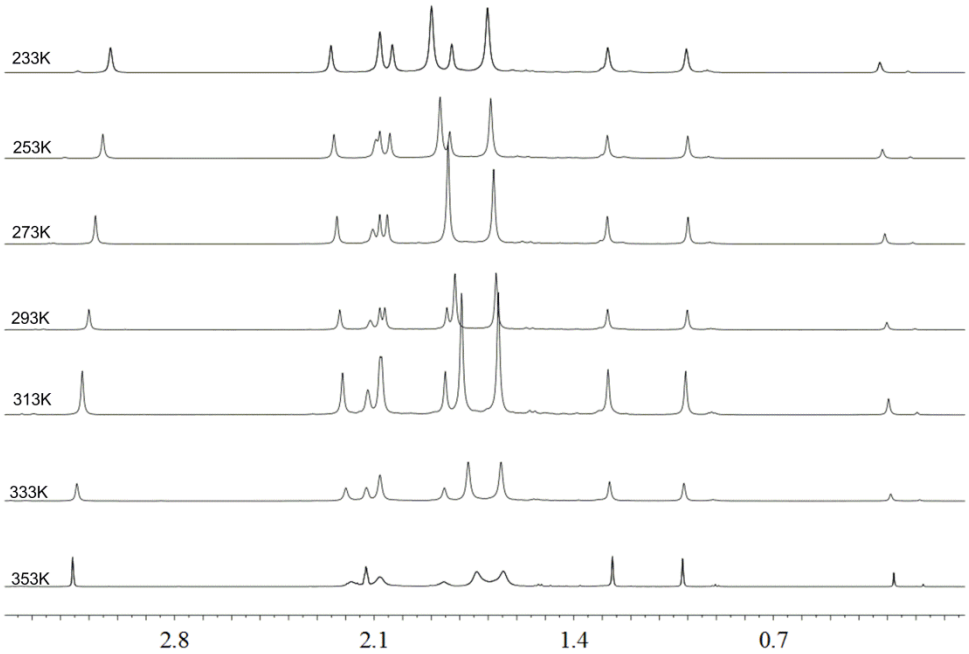

Figure S27. The variable temperature ^{1}H NMR spectra of complex **10**: A) the whole spectra; B) partial signals are shown (400 MHz, toluene-d_8).

A)

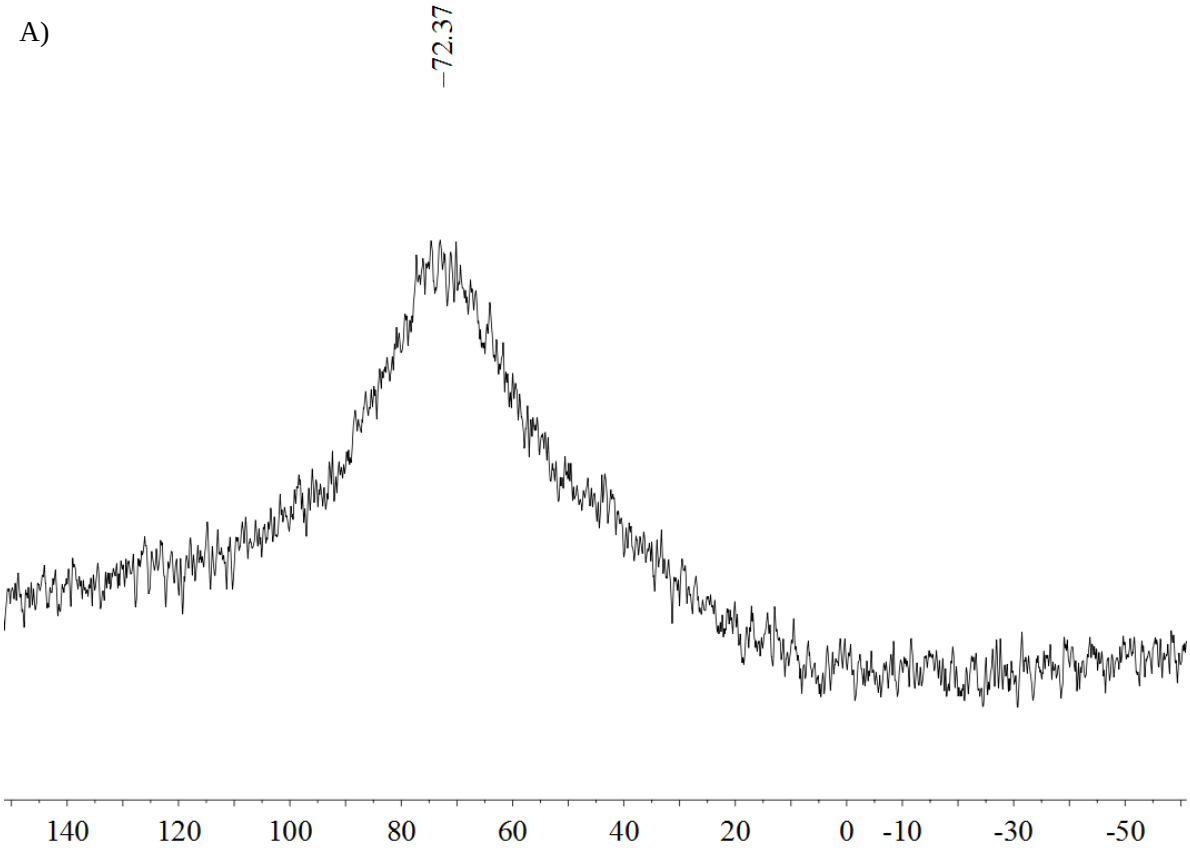

B)

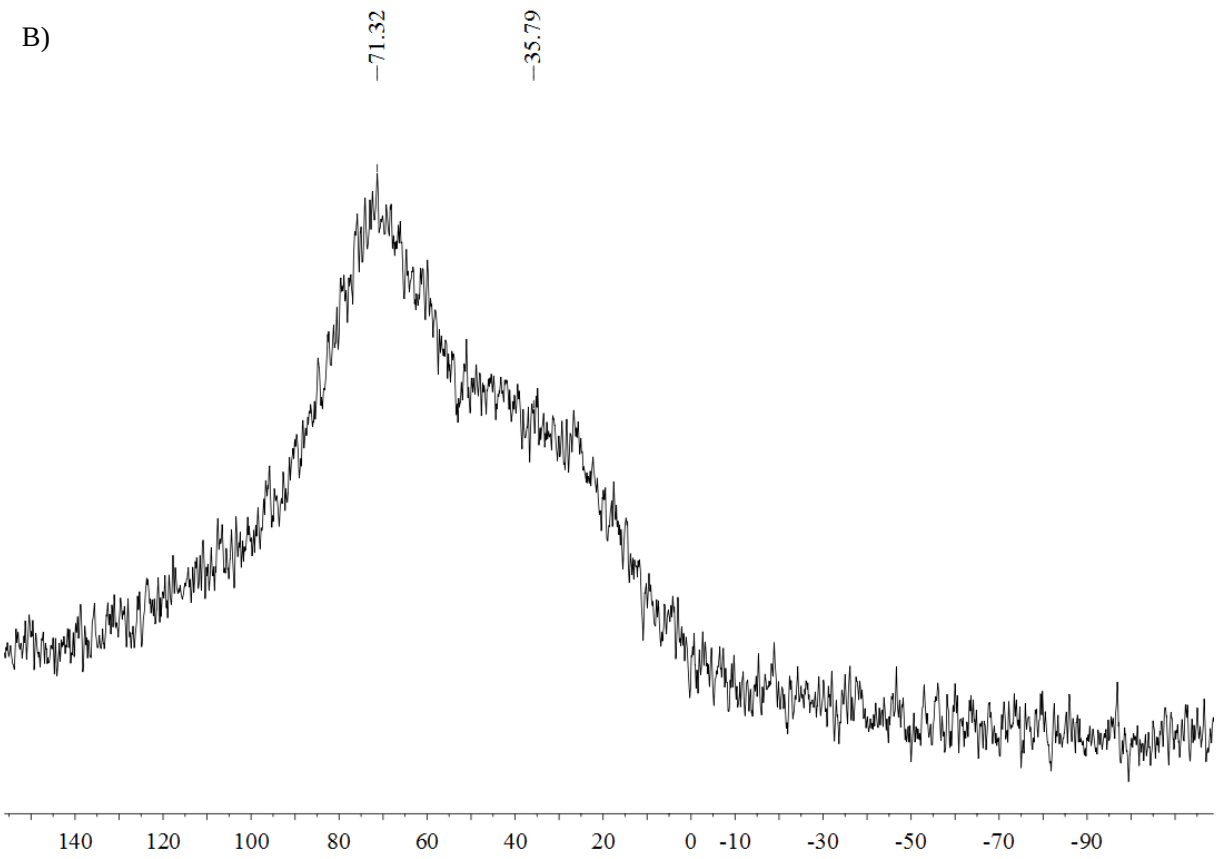

Figure S28. ^{27}Al NMR spectrum of A) complex **5**; B) complex **10** (130.3 MHz, $CDCl_3$, r.t.).

4. NMR studies

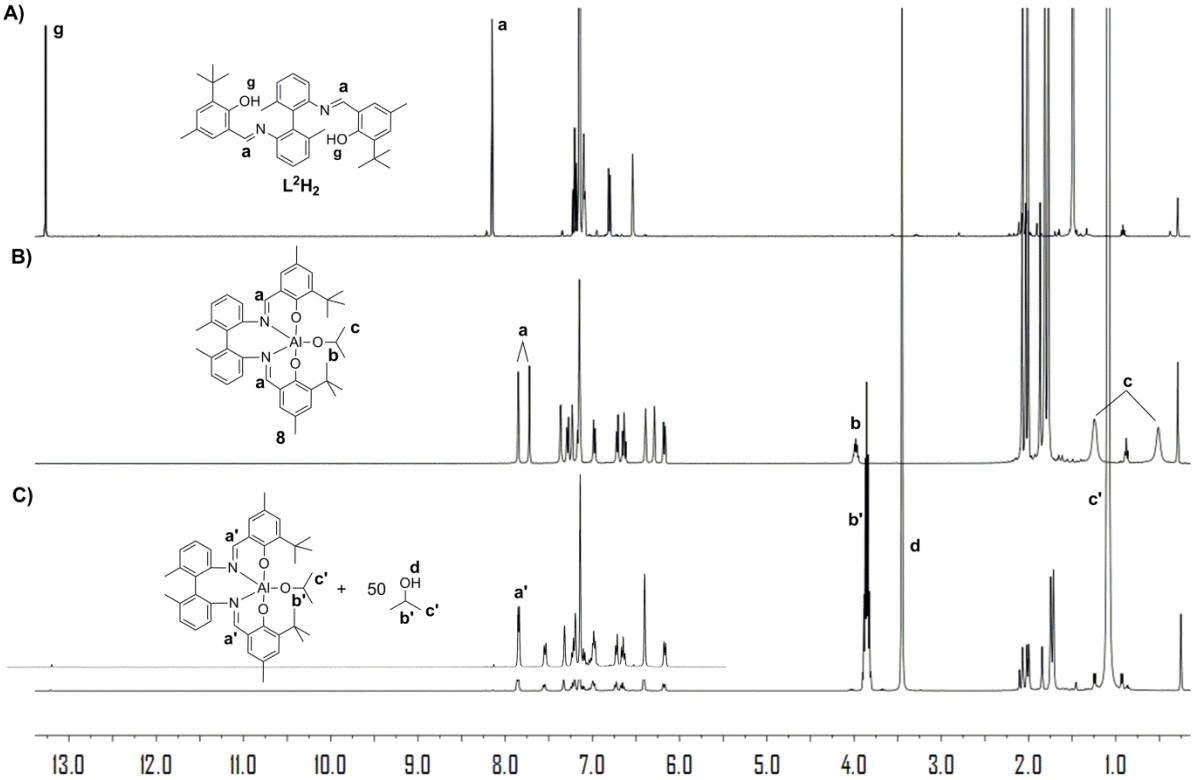

Figure S29. ^{1}H NMR spectra of A) proligand; B) complex **8**; C) the reaction mixture of complex **8** and 50 equiv. of ^{i}PrOH (C_6D_6, 400 MHz, r.t).

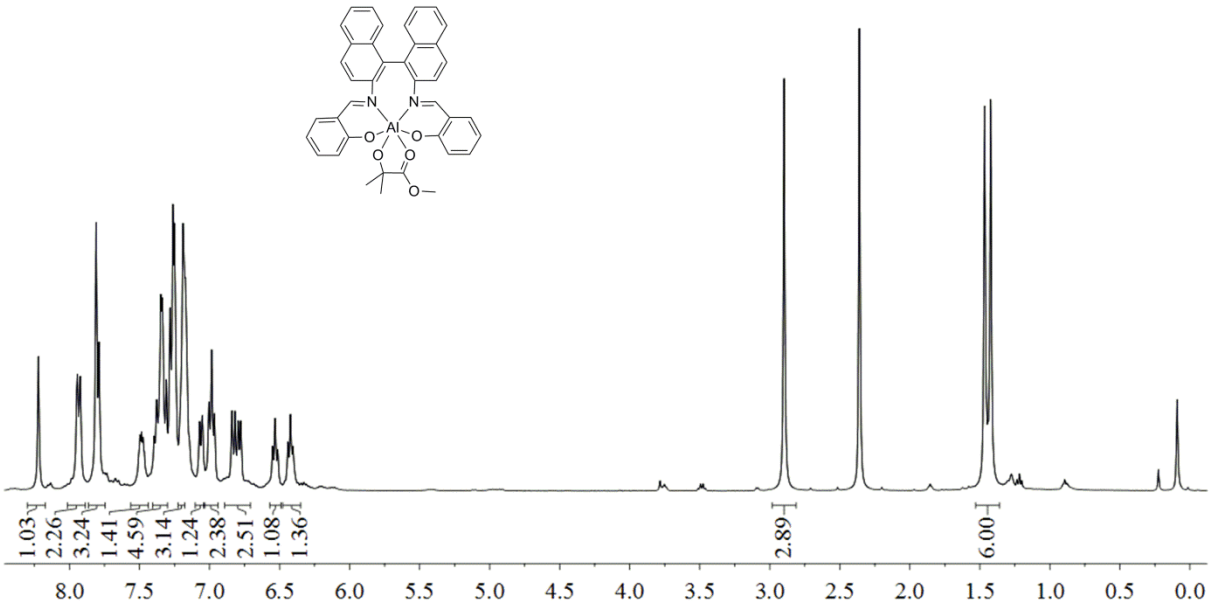

Figure S30. ^{1}H NMR spectrum of the reaction mixture of *rac*-(SalBinap)AlMe and methyl 2-hydroxyisobutyrate (400 MHz, $CDCl_3$, r.t.).

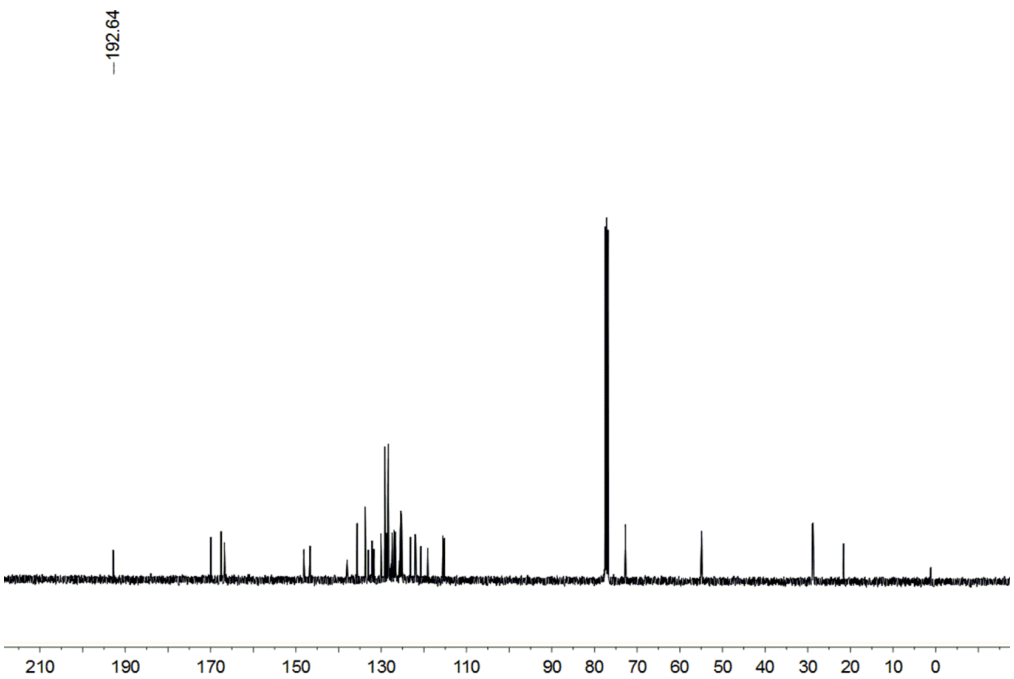

Figure S31. ^{13}C NMR spectrum of the reaction mixture of *rac*-(SalBinap)AlMe and methyl 2-hydroxyisobutyrate (100 MHz, $CDCl_3$, r.t.).

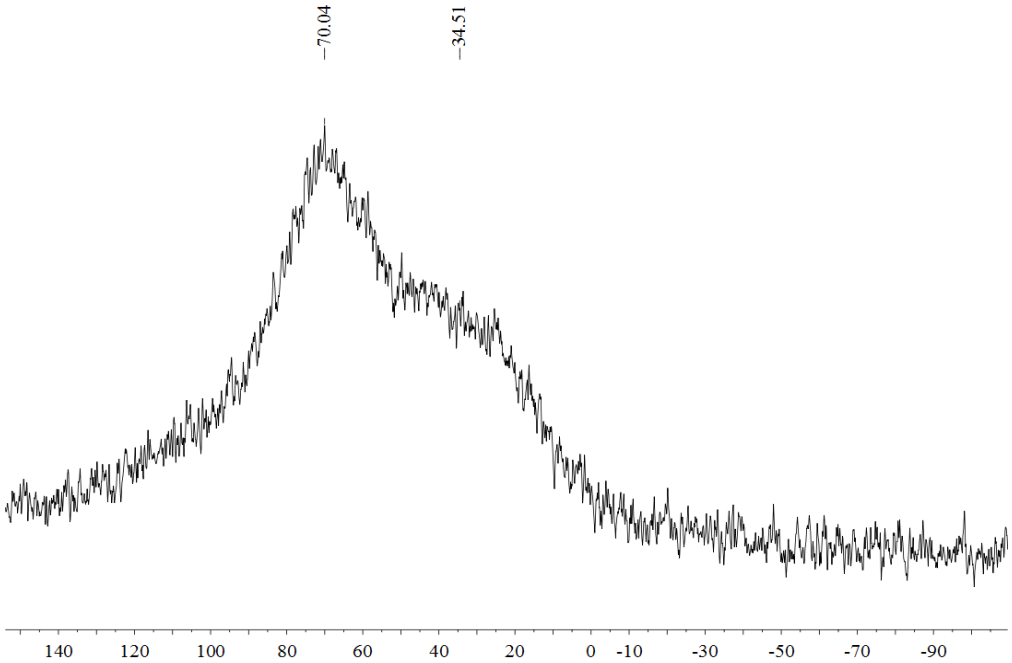

Figure S32. ^{27}Al NMR spectrum of the reaction mixture of *rac*-(SalBinap)AlMe and methyl 2-hydroxyisobutyrate ($CDCl_3$, 130.3 MHz, r.t).*

* The extremely low symmetric property around the Al center led to the weak singnal in ^{27} Al NMR in Figure S28 and S32, when even more than 100 mg complex was added to the NMR tube and detected for about 10 hours. ([a] N. Nomura, T. Aoyama, R. Ishii and T. Kondo, *Macromolecules*, 2005, **38**, 5363−5366; [b] H. Du, A. H. Velders, P. J. Dijkstra, J. Sun, Z. Zhong, X. Chen and J. Feijen, *Chem. Eur. J.*, 2009, **15**, 9836−9845.)

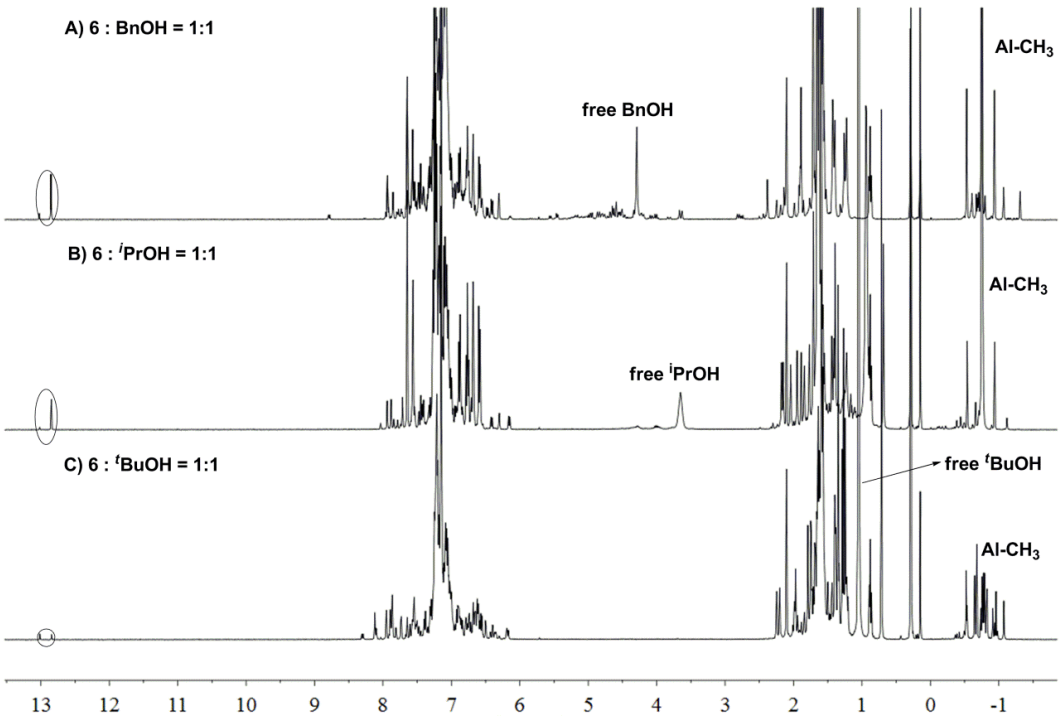

Figure S33. ^{1}H NMR spectra of the NMR tube reactions between complex **6** and A) BnOH, determined immediately after mixing; B) ^{i}PrOH, determined immediately after mixing; C) ^{t}BuOH, determined after mixing for 12 h at 80 ^{o}C (All in C_6D_6, 400 MHz, r.t.).

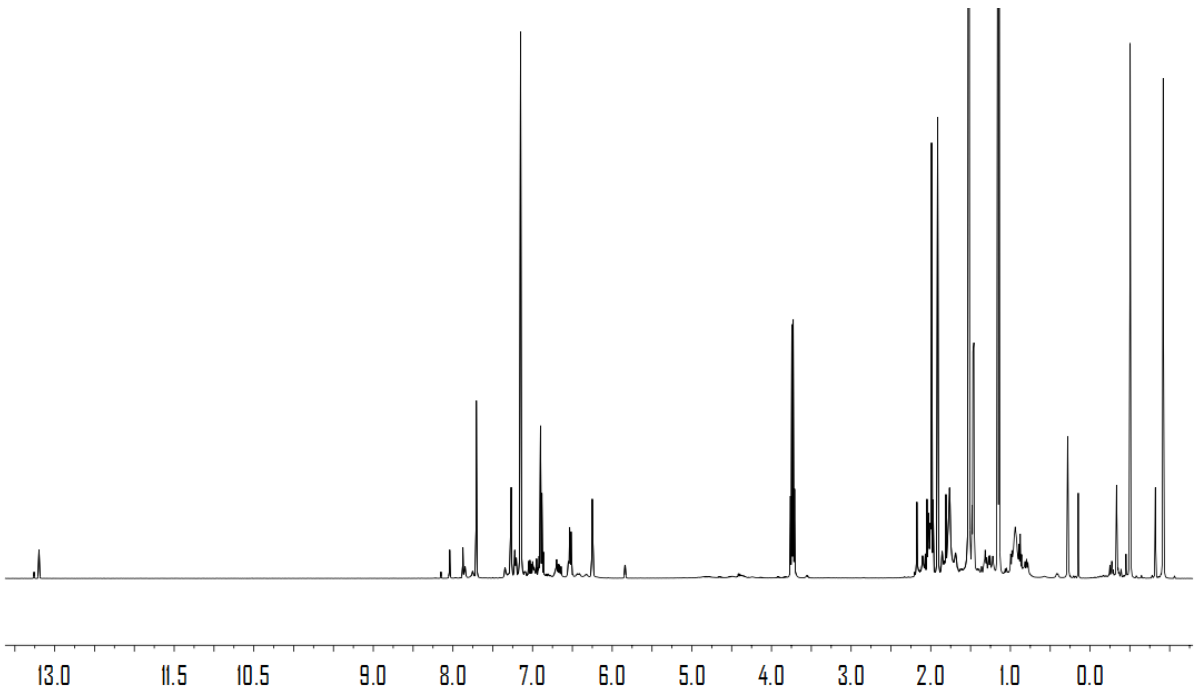

Figure S34. ^{1}H NMR spectrum of the NMR tube reactions of complex **5** and one equiv. of ^{i}PrOH in the presence of 20 equiv. of *rac*-LA (C_6D_6, 400 MHz, r.t.).

5. Kinetic studies

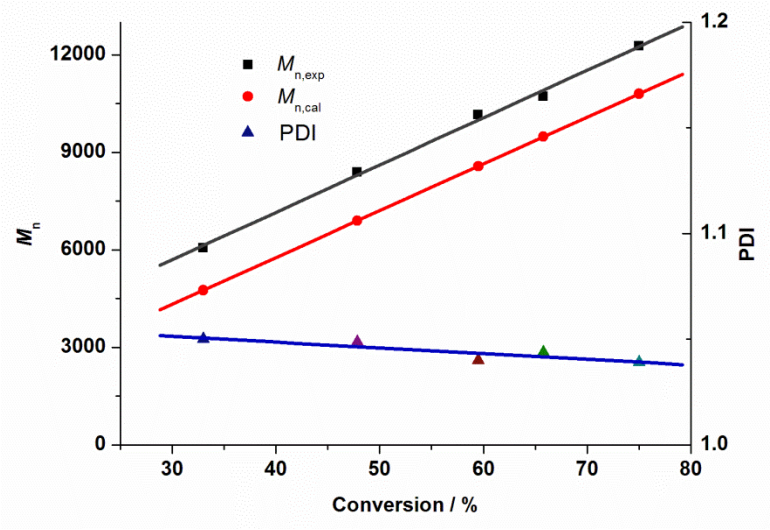

Figure S35. Relationship of M_n and the polydispersity index (PDI) of the PLA samples versus monomer conversion obtained by complex **2** ([*rac*-LA]$_0$ = 1.0 M, [*rac*-LA]$_0$: [**2**]$_0$: [^{i}PrOH]$_0$ = 100:1:1, 110 ℃, in toluene).

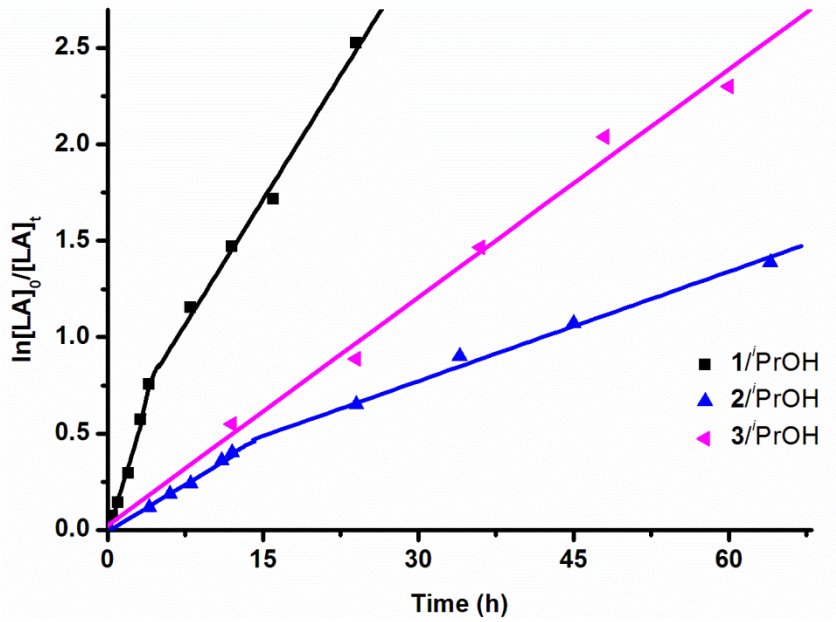

Figure S36. Semilogarithmic plots for the polymerization of *rac*-LA initiated by complexes **1**–**3**/^{i}PrOH. ([*rac*-LA]$_0$: [Al]$_0$: [^{i}PrOH]$_0$ = 100:1:1, [*rac*-LA]$_0$ = 1.0 M, 110 ^{o}C, toluene) For **1**, first stage, k_{app} = (18.9 ± 1.5) × 10^{-2} h^{-1}, R = 0.990; second stage, k_{app} = (8.60 ± 0.39) × 10^{-2} h^{-1}, R = 0.997. For **2**, first stage, k_{app} = (3.23 ± 0.18) × 10^{-2} h^{-1}, R = 0.996; second stage, k_{app} = (1.89 ± 0.12) × 10^{-2} h^{-1}, R = 0.996. For **3**, k_{app} = (3.94 ± 0.18) × 10^{-2} h^{-1}, R = 0.996.

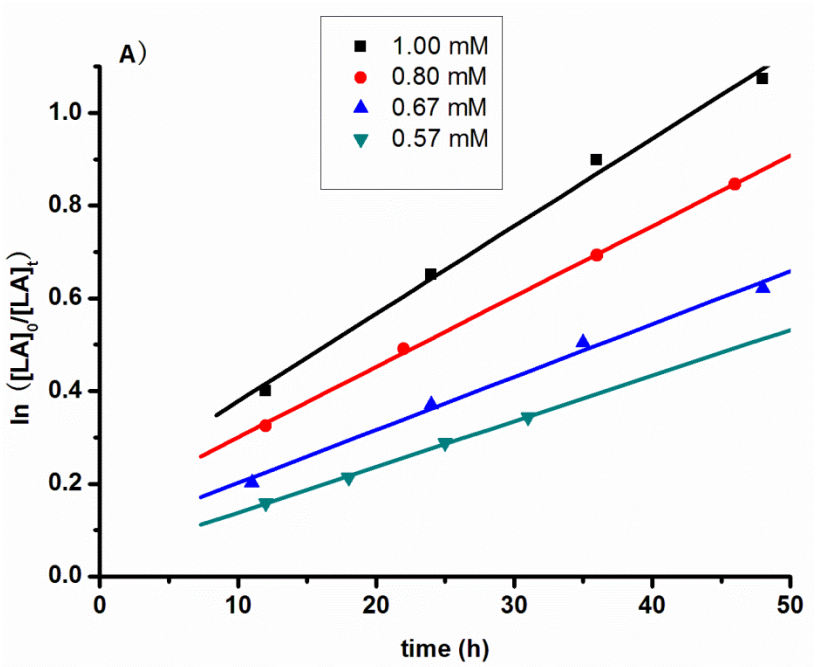

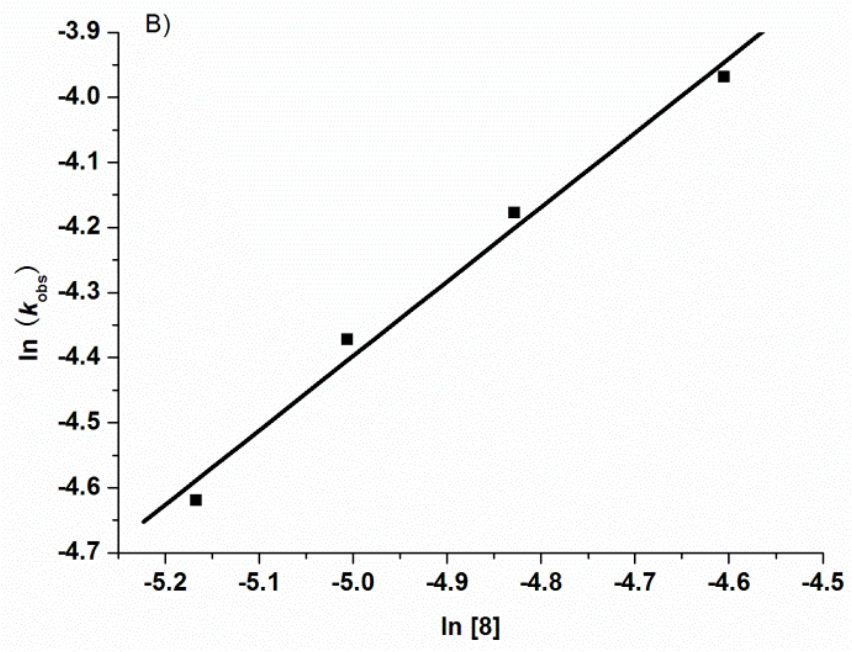

Figure S37. A) Linear plots of ln([LA]$_0$/[LA]$_t$) versus time; B) Linear plot of ln k_{obs} versus ln[Al] for the polymerization of *rac*-LA using **8** as an initiator ([*rac*-LA]$_0$ = 1.0 M; [Al]$_0$ = 0.01, 0.008, 0.0067, 0.0057 M in toluene at 110 ℃).

6. Microstructure analysis of polylactides

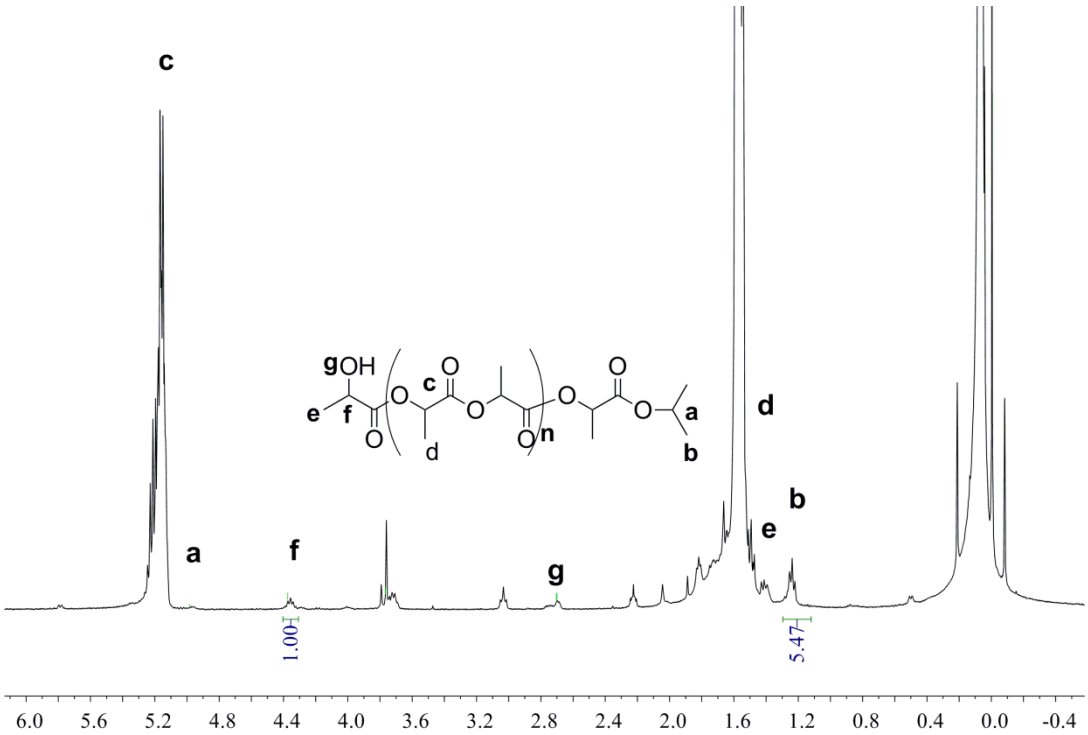

Figure S38. ^{1}H NMR spectrum (400 MHz, $CDCl_3$) of *rac*-LA oligomer produced by complex **8** ([*rac*-LA]$_0$: [**8**]$_0$ = 20:1, in toluene).

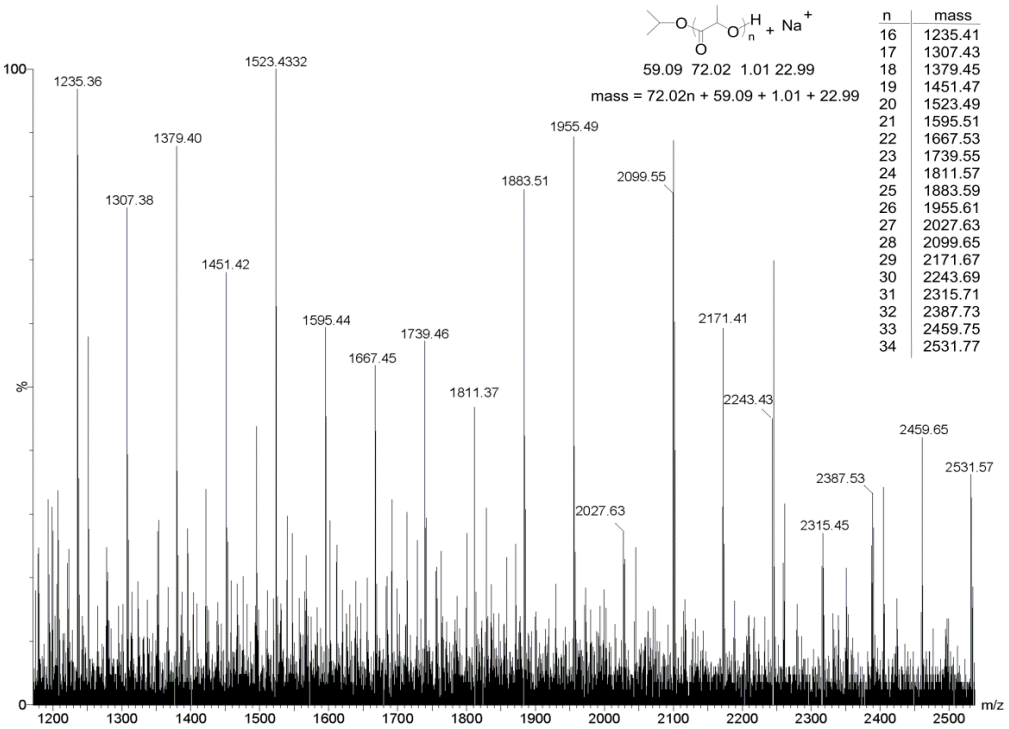

Figure S39. ESI-TOF mass spectrum of the *rac*-LA oligomer produced by complex **8** ([*rac*-LA]$_0$: [**8**]$_0$ = 20:1, in toluene).

Peak	Integration	P_m
sis	0.062	0.65
sii	0.103	0.71
iis	0.091	0.76
iii	0.646	0.74
isi	0.098	0.80
	Average	0.73

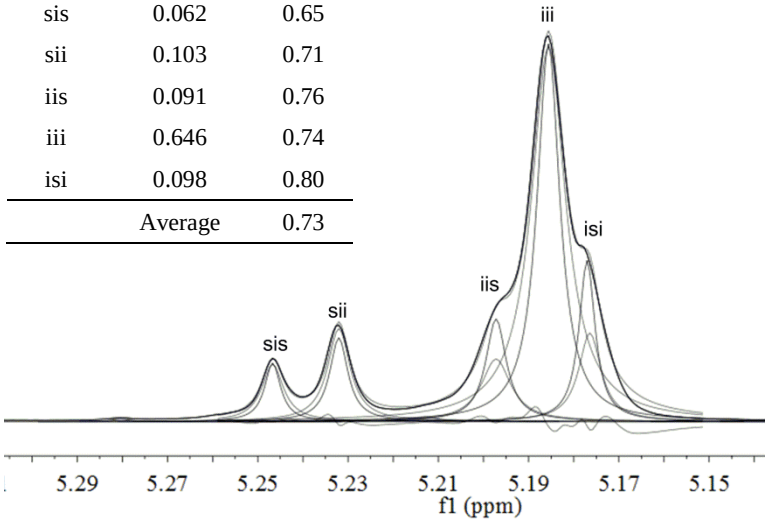

Figure S40. Homonuclear decoupled ^{1}H NMR spectrum (400 MHz, $CDCl_3$) of PLA produced from *rac*-LA using complex **1**/^{i}PrOH as initiator ([*rac*-LA]$_0$ = 1.0 M, [*rac*-LA]$_0$: [**1**]$_0$: [^{i}PrOH]$_0$ = 100:1:1, in toluene, 110 ^{o}C, 92% monomer conversion, P_m = 0.73).

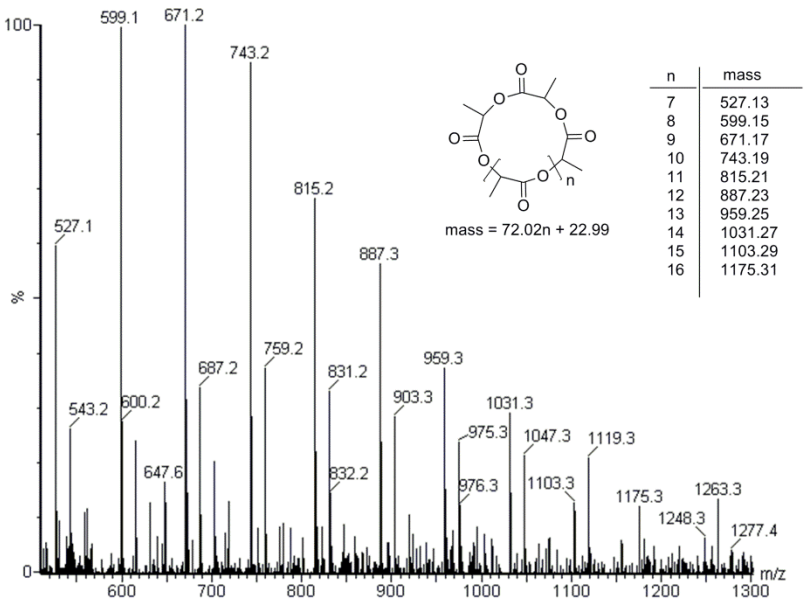

Figure S41. ESI-TOF mass spectrum of the *rac*-LA oligomer produced by complex **4** ([*rac*-LA]$_0$: [**4**]$_0$ = 20:1, in toluene).

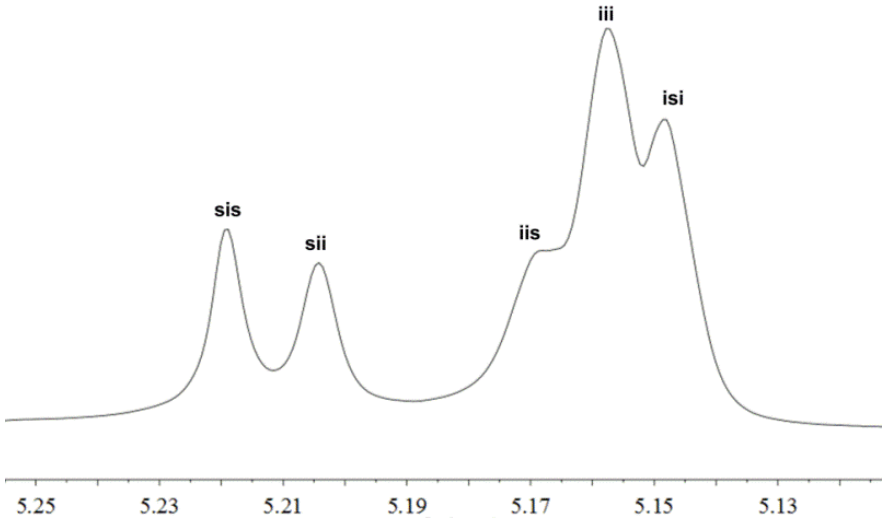

Figure S42. Homonuclear decoupled ^{1}H NMR spectrum of PLA produced from *rac*-LA using complex **4** as initiator ([*rac*-LA]$_0$ = 1.0 M, [*rac*-LA]$_0$: [**4**]$_0$ = 100:1, in toluene, 110 ^{o}C, 90% monomer conversion, P_m = 0.56).